

# High Energy $\gamma$ -rays From FR I Jets

L. Stawarz

*Obserwatorium Astronomiczne, Uniwersytet Jagielloński,  
ul. Orła 171, 30-244 Kraków, Poland*

stawarz@oa.uj.edu.pl

M. Sikora

*Centrum Astronomiczne im. M. Kopernika,  
ul. Bartycka 18, 00-716 Warszawa, Poland  
also at Stanford Linear Accelerator Center, Stanford, CA 94309-4349*

and

M. Ostrowski

*Obserwatorium Astronomiczne, Uniwersytet Jagielloński,  
ul. Orła 171, 30-244 Kraków, Poland  
also at Stanford Linear Accelerator Center, Stanford, CA 94309-4349*

## ABSTRACT

Thanks to *Hubble* and *Chandra* telescopes, some of the large scale jets in extragalactic radio sources are now being observed at optical and X-ray frequencies. For the FR I objects the synchrotron nature of this emission is surely established, although a lot of uncertainties – connected for example with the particle acceleration processes involved – remain. In this paper we study production of high energy  $\gamma$ -rays in FR I kiloparsec-scale jets by inverse-Compton emission of the synchrotron-emitting electrons. We consider different origin of seed photons contributing to the inverse-Compton scattering, including nuclear jet radiation as well as ambient, stellar and circumstellar emission of the host galaxies. We discuss how future detections or non-detections of the evaluated  $\gamma$ -ray fluxes can provide constraints on the unknown large scale jet parameters, i.e. the magnetic field intensity and the jet Doppler factor. For the nearby sources Centaurus A and M 87, we find measurable fluxes of TeV photons resulting from synchrotron self-Compton process and from comptonisation of the galactic photon fields, respectively. In the case of Centaurus A, we also find a relatively strong emission component due to comptonisation of the nuclear blazar photons, which could be easily observed by *GLAST* at energy  $\sim 10$  GeV, providing important test for the unification of FR I sources with BL Lac objects.

*Subject headings:* radiation mechanisms: nonthermal—galaxies: jets—galaxies: individual (Centaurus A, M 87)—gamma rays: theory

## 1. Introduction

$\gamma$ -rays are detected from many galactic and extragalactic sources, including pulsars, supernova remnants, gamma ray bursts and blazars. It is believed that multiwavelength emission of the latest type of the mentioned objects is due to small scale highly relativistic jets, which are formed near active galactic nuclei of host galaxies and are inclined at small angles to the line of sight (e.g., Bregman 1990). High observed bolometric luminosities of blazars (typically  $10^{44} - 10^{48}$  erg/s) are often dominated by  $\gamma$ -ray emission, what enabled to observe many of them by *EGRET* in  $\varepsilon_\gamma \sim 0.1 - 10$  GeV energy range (von Montigny et al. 1995; Hartman et al. 1999). Some nearby low-luminosity blazars, like the best known Mrk 421 and Mrk 501, are also confirmed to be sources of very high energy (VHE)  $\gamma$ -rays with  $\varepsilon_\gamma > 100$  GeV (Punch et al. 1992; Quinn et al. 1996, respectively). Detection of such VHE radiation by ground-based instruments was possible due to development of imaging atmospheric Cherenkov telescopes, *IACTs* (see, e.g., Aharonian 1998; Völk 2003).

The observed broad-band blazar emission allows one to determine physical parameters of nuclear AGN jets.  $\gamma$ -ray observations are crucial in this respect, providing important constraints on the involved particle acceleration processes, or on the characteristic spatial scales for the blazar phenomenon (e.g., Sikora and Madejski 2002; Kino et al. 2002). However, observations at VHE range are complicated because propagation effects are important for the high energy photons created at cosmological distances (Nikishov 1962; Gould and Schreder 1966; Stecker et al. 1992), and also, obviously, because of a low photon statistics in  $\gamma$ -ray telescopes. Among the other issues, one should mention here a case of VHE emission from Mrk 501, which extends up to energies  $\varepsilon_\gamma > 10$  TeV, which seems to be in conflict with some models of cosmic infrared background (CIB) radiation (see, e.g., Protheroe and Meyer 2000; Aharonian 2001). Detailed studies of cosmic background photon fields and their interactions with  $\gamma$ -rays during their propagation, as well as future  $\gamma$ -ray missions, will possibly answer some of the questions connected with production of VHE radiation in blazars.

Contrary to blazar parsec-scale jets, their large scale counterparts extending from a few to a few hundreds of kiloparsecs from active galactic nuclei were usually studied only at radio frequencies (Bridle and Perley 1984). Recently, however, *Hubble* (*HST*) and *Chandra* telescopes gathered new information about optical and X-ray emission of some of these objects. For several hundreds of known radio jets, only about 20 are observed at optical

frequencies<sup>1</sup>. Most of them are relatively short and faint, with only a few exceptions like the one in M 87 allowing for detailed spectroscopic and morphological studies (Meisenheimer et al. 1996; Perlman et al. 1999, 2001). Surprisingly, the large scale jets can be also very prominent in X-rays. Up to now, more than 20 jets were detected by *Chandra* within the 1 – 10 keV energy range<sup>2</sup>, although the nature of this emission is still under debate (e.g., Tavecchio et al. 2000; Bai and Lee 2001; Celotti et al. 2001; Aharonian 2002; Carilli et al. 2002; Harris and Krawczynski 2002; Stawarz and Ostrowski 2002; Sahayanathan et al. 2003; Tavecchio et al. 2003). In general, both optical and X-ray observations question in many aspects the standard models for the extragalactic jets emission.

As the large scale jets in radio galaxies are confirmed sources of optical and X-ray photons, one can ask if they can be also observed at  $\gamma$ -ray energies. Such observations could impose significant constraints on jet parameters (in analogy to the blazar sources), as well as for the unification scheme of radio-loud AGNs. In the present paper we make predictions regarding production of high energy  $\gamma$ -rays in FR I jets by the inverse-Compton scattering in a framework of one electron population model. In discussion, we refer to the objects observed by *Chandra*, as the X-ray observations of these recently widely studied sources impose important constraints on the jet synchrotron emission, crucial in determining the high energy photon flux. We find, that for the jet parameters inferred from radio-to-X-ray observations, only nearby Centaurus A and M 87 jets are expected to be observed at GeV – TeV energies by near future  $\gamma$ -ray missions (cf. discussion in section 3). However, it is possible that more distant objects will be also detected, if the unconstrained jet parameters (like magnetic field and kinematic factors) differ from typically assumed values (sections 2.3.1 – 2.3.3).

The already mentioned propagation effects can seriously affect the observed VHE spectra of distant objects, as interaction of VHE  $\gamma$ -rays with the CIB photon field is expected to result in their efficient absorption due to photon-photon pair creation. CIB radiation is created by infrared emission of forming stars in early cosmological epochs and the following reprocessing by ambient dust. The origin, evolution and detailed energy distribution of CIB are still uncertain, mostly because of observational difficulties (for a recent review see Hauser and Dwek 2001). The existing controversies, particularly important in a TeV-absorption range (at  $\nu_{CIB} \sim 10^{13}$  Hz) are however not crucial for our discussion, as we limit ourselves to relatively close object. For illustration, we refer to work by Kneiske et al. (2002, and references therein) who, among the others, studied opacity of the Universe to  $\gamma$ -rays and

---

<sup>1</sup>see homepage <http://home.fnal.gov/~jester/optjets> by S. Jester and references therein

<sup>2</sup>see homepage <http://hea-www.harvard.edu/XJETS> by D. Harris and references therein

evolution of the diffusive infrared-to-ultraviolet background radiation field.

Below, in section 2, based on optical and X-ray observations we reconstruct and comment ‘typical’ electron energy distribution of FR I *Chandra* jets. We estimate different photon fields contributing to the inverse-Compton scattering of these electrons, and next evaluate and discuss the resulting fluxes and photon break energies in the Thomson regime. Section 3 contains detailed analysis of the  $\gamma$ -ray emission from the nearby sources Centaurus A and M 87. Final conclusions are presented in section 4.

## 2. Emission from the large scale jets in FR I sources

### 2.1. Synchrotron emission: radio-to-X-rays

*Chandra* X-ray observatory detected about 10 jets displaying the FR I large scale morphology. They include the ones in radio galaxies M 87 (Marshall et al. 2002; Wilson and Yang 2002), Centaurus A (Kraft et al. 2000, 2002), 3C 129 (Harris et al. 2002a), 3C 31 (Hardcastle et al. 2002), PKS 0521-365 (Birkinshaw et al. 2002), 3C 270 (Chiaberge et al. 2003), M 84 (Harris et al. 2002b), 3C 66B (Hardcastle et al. 2001), B2 0206+35 and B2 0755+37 (Worrall et al. 2001). All of these objects are located relatively nearby, with a distance ranging from 3.4 Mpc (Centaurus A) to more than 300 Mpc (PKS 0521-315 at redshift  $z = 0.055$ ). All of them share many spectral and morphological similarities briefly summarised below.

X-ray jets in FR I radio sources are usually quite short (projected length  $\sim 1 - 4$  kpc). Typically, they are composed of diffusive knots with a spatial scale  $R \sim 0.1$  kpc, although a strong inter-knot emission is also sometimes present. X-ray jet morphology corresponds *roughly* to the radio morphology, and – in cases of M 87, PKS 0521-315, 3C 66B, 3C 31 and B2 0755+37 observed by *HST* – to the optical one. A noted difference between these pictures are spatial offsets of some knot maxima as measured at X-rays and at radio/optical frequencies (up to  $\sim 0.008$  kpc in M 87,  $\sim 0.08$  kpc in Centaurus A and  $\sim 0.2$  kpc in 3C 66B). Also, X-ray jets (knots) seem to be narrower than their radio/optical counterparts (M 87, Centaurus A). Except of the weakest and the smallest objects (3C 270 and M 84), the observed X-ray luminosities of the discussed jets are  $L_X \sim 10^{39} - 10^{42}$  erg/s.

In most cases, multiwavelength observations of knot regions in FR I *Chandra* jets allow one to construct broad band radio-to-X-ray spectral energy distribution. All of the inferred knot spectra seem to be similar, and in addition difficult to be explained in a framework of standard jet models. A spectral index of the radio emission (defined in a way  $S_\nu \propto \nu^{-\alpha}$ , where  $S_\nu$  is the energy flux spectral density) is always close to  $\alpha_R \sim 0.6$ . The optical emission obviously belongs to the synchrotron continuum, with the spectral index steepening between

infrared and optical frequencies at about  $\Delta\alpha \sim 0.7$  (3C 66B, PKS 0521-315, M 87). This agrees well with the X-ray spectral index measured by *Chandra*, which, for FR I jets, is on average  $\alpha_X \sim 1.3$  (ranging from  $\sim 1.1$  in 3C 31 to  $\geq 1.5$  in some knots of M 87 and Centaurus A). Thus, one can generalize, that in the discussed objects the radio-to-optical power-law slope is always less than unity ( $\alpha_{RO} \sim 0.5 - 0.8$ ), while the optical-to-X-ray power-law slope is always much larger ( $\alpha_{OX} \sim 1.1 - 1.5$ ). Such spectral behaviour seems to be universal for all FR I X-ray jets, with a spectral break (*br*) – where most of the synchrotron (*syn*) power is emitted – placed usually around  $\nu_{syn,br} \sim 10^{14}$  Hz or, eventually (M 87), at higher frequencies.

The steep X-ray spectral indices of FR I large scale jets exclude an inverse-Compton scattering as a mechanism responsible for the observed X-ray emission. Instead, radio-to-X-ray spectral properties indicate synchrotron origin of detected 1 – 10 keV photons. If this is the case, than in the discussed objects unknown acceleration process operates, which results in characteristic and *universal* for FR I jets electron energy distribution which can be approximated as a broken power-law:

$$n'_e(\gamma) \propto \begin{cases} \gamma^{-p} & \text{for } \gamma_0 < \gamma < \gamma_{br} \\ \gamma^{-(p+2\Delta\alpha)} & \text{for } \gamma_{br} < \gamma < \gamma_{max} \end{cases}, \quad (1)$$

where  $\gamma$  is the electron Lorentz factor<sup>3</sup>,  $\Delta\alpha$  is the spectral break in the synchrotron continuum and  $p = 2\alpha_R + 1 \sim 2.2$ . Optical and X-ray observations play a crucial role in determining parameters of the above electron spectrum, i.e. its normalisation (for the assumed energy equipartition between electrons and the jet magnetic field) and the actual values of  $\gamma_{br}$  and  $\gamma_{max}$ , which in turn determine the inverse-Compton  $\gamma$ -ray jet radiative output. For non-relativistic jet velocities, a typical  $\nu_{syn,br} \sim 10^{14} - 10^{15}$  Hz and an equipartition magnetic field  $B \sim 10^{-4}$  G, one gets  $\gamma_{br} \sim 10^5 - 10^6$  and  $\gamma_{max} > 10^7$ . Discussion of the acceleration processes creating such high energy electrons in the FR I jets is beyond the scope of this paper. Let us note however, that it is possible for  $n'_e(\gamma)$  to possess a more complicated form than the one given by equation 1, involving for example spectral pile-ups at the maximum electron energies due to efficient electron acceleration and rapid radiative cooling (Dermer and Atoyan 2002; Stawarz and Ostrowski 2002). In either case, as the observed X-ray luminosity of the FR I kpc-scale jets is lower than the optical luminosity, most of the electrons energy is concentrated in the range near the electron break Lorentz factor  $\gamma_{br}$ .

---

<sup>3</sup>Hereafter we follow the notation with the primed quantities measured in the jet comoving frame and the bare ones if given in the observer rest frame (neglecting cosmological corrections). However, we do not prime the magnetic field induction  $B$  as well as electron Lorentz factors  $\gamma$ , noting instead that they always refer to the emitting plasma rest frame.

It is interesting to compare  $\nu_{syn,br}$  characteristic for the kpc-scale FR I jets with critical ( $cr$ ) synchrotron frequency  $\nu_{syn,cr}$  resulting from the interplay between electron synchrotron cooling and dynamical evolution of the emitting region. The time scale for the former process can be estimated as  $t'_{loss} \sim \gamma/|\dot{\gamma}|_{syn}$ , where  $mc^2 |\dot{\gamma}|_{syn} = \frac{4}{3} c \sigma_T U'_B \gamma^2$  is a mean rate of electron energy losses due to synchrotron emission, and  $U'_B = B^2/8\pi$  denotes comoving jet magnetic field energy density. The second time scale is simply  $t'_{dyn} = t_{dyn}/\Gamma \sim r/c\Gamma$ , where  $\Gamma = (1 - \beta^2)^{-1/2}$  is the jet bulk Lorentz factor,  $\beta c$  is a jet bulk velocity and  $r$  is the distance of the kpc-scale structure from the jet base at  $r_0 \ll r$  from the active galactic nucleus. A critical electron Lorentz factor is defined by an equality  $t'_{dyn} \approx t'_{loss}(\gamma = \gamma_{cr})$ . Thus, assuming initial injection of the power-law electron energy distribution at  $r_0$ , one expects that at the distance  $r$  the electron spectrum steepens for  $\gamma > \gamma_{cr}$  because of the efficient radiative cooling of these electrons. The observed critical synchrotron frequency is then  $\nu_{syn,cr} = \nu'_{syn,cr} \delta \propto \gamma_{cr}^2 B \delta$ , where

$$\delta = \frac{1}{\Gamma(1 - \beta \cos \theta)} \quad (2)$$

is the jet Doppler factor and  $\theta$  is the jet inclination angle to the line of sight. Assuming that the jet magnetic field scales with the distance as  $B = B_0(r_0/r)$ , what conserves the Poynting flux  $L'_B \propto R^2 U'_B$  in the expanding jet with an opening angle  $\varphi \sim const$  and a radius  $R \sim \varphi r$ , one obtains

$$\nu_{cr} \sim 4 \cdot 10^{14} r_1 \delta \Gamma^2 \quad \text{Hz} \quad , \quad (3)$$

where we put  $r_0 = 1$  pc,  $B_0 = 0.1$  G and  $r_1 \equiv r/1$  kpc. Note, that with the above values of  $B_0$  and  $r_0$  characteristic for the blazar sources, the kpc-scale jet magnetic field is expected to be  $B \sim 10^{-4}$  G, consistently with the equipartition value. Hence, in a case of a non-relativistic kpc-scale jet velocity,  $\nu_{syn,cr} \sim \nu_{syn,br} \sim 10^{14}$  Hz. However, the spectral break resulting from the considered process is  $\Delta\alpha_{cr} = 0.5$  (Kardashev 1962), i.e. slightly less than the one required for the FR I *Chandra* jets. Possibly, the observed steep spectral break is a signature of the electron synchrotron cooling in the spatially *inhomogeneous* magnetic field (Cavallo et al. 1980; Coleman and Bicknell 1988). Note also, that in the cases of relativistic jet bulk velocities, the observed value of  $\nu_{syn,cr}$  can be significantly higher than  $10^{14}$  Hz (cf. the case of M 87, section 3.2).

Radio observations of FR I jets indicate moderate or even weak beaming (e.g., Laing et al. 1999). However, one cannot exclude possibility that the bulk Lorentz factors of kpc-scale jets in weak radio galaxies are of order of a few. This idea is supported by *HST* observations of superluminal motions and *Chandra* detection of significant X-ray variability at kpc-scales in M87 (Biretta et al. 1999; Harris et al. 2003, respectively). In fact, a small number of

detected optical and X-ray jets in radio galaxies as compared to the number of known radio jets suggests that relativistic beaming effects can play an important role in these sources (Sparks et al. 1995; Scarpa and Urry 2002; Jester 2003). Including a relativistic correction, the electron break Lorentz factor is

$$\gamma_{br} \sim 5 \cdot 10^5 \left( \frac{\nu_{syn,14}}{B_{-4} \delta} \right)^{1/2}, \quad (4)$$

where  $\nu_{syn,14} \equiv \nu_{syn,br}/10^{14}$  Hz and  $B_{-4} \equiv B/10^{-4}$  G.

## 2.2. Radiation fields within the kpc-scale jet

Let us consider a kpc-scale ( $r \sim 1 - 4$  kpc) relativistic jet with the bulk Lorentz factor  $\Gamma$ , inclined at an angle  $\theta$  to the line of sight. The energy density of the jet magnetic field, as measured in the emitting region rest frame, is

$$U'_B = \frac{B^2}{8\pi} \sim 4 \cdot 10^{-10} B_{-4}^2 \text{ erg cm}^{-3}. \quad (5)$$

As mentioned above, the equipartition value inferred from the synchrotron emission of FR I knot regions is typically  $B_{eq} \sim 10^{-4}$  G, and it corresponds to the observed synchrotron jet luminosities  $L_{syn} \sim 10^{40} - 10^{42}$  erg/s. The observed luminosity is related to the total emitted synchrotron power  $L'_{syn}$  by the relation

$$L_{syn} = g_{cj/mb}(\Gamma, \theta) L'_{syn}, \quad (6)$$

where

$$g_{cj/mb}(\Gamma, \theta) = \begin{cases} \delta^3/\Gamma & (cj) \\ \delta^4 & (mb) \end{cases} \quad (7)$$

in cases of a continuous jet (*cj*) or a moving single radiating blob (*mb*), respectively (Sikora et al. 1997, see also Appendix A)<sup>4</sup>. Below we analyse these both possibilities as limiting models for the kpc-scale knots. We also consider synchrotron luminosity at a given break frequency  $\nu_{syn,br}$ , hereafter denoted as  $[\nu L_\nu]_{syn,br}$ , rather than the bolometric one  $L_{syn}$ , with transformations between  $[\nu L_\nu]_{syn,br}$  and  $[\nu' L'_{\nu'}]_{syn,br}$  the same as given in equations 6 - 7. For the broken power-law synchrotron spectrum assumed here, with  $\alpha \sim 0.6$  and  $\Delta\alpha \sim 0.7$  (cf. equation 1) one has a bolometric correction  $L_{syn}/[\nu L_\nu]_{syn,br} \approx 6$ .

---

<sup>4</sup>Note, that as discussed in Appendix A, in both cases the equipartition magnetic field measured in the emitting region rest frame is related to the equipartition value computed for no beaming by the relation  $B_{eq} = B_{eq, \delta=1} \delta^{-5/7}$ .

In addition to the synchrotron emission extending to the X-rays, the FR I jets produce also the high energy radiation by inverse-Compton scattering of ambient photon fields, like, for example, the cosmic microwave background (CMB) radiation or the synchrotron emission produced by the jet itself. At the kiloparsec distances from the galactic center another important sources of ambient photons are the active galactic nucleus and the host galaxy. The AGN radiation, produced at small distances from the central region, illuminates the large scale jet almost exactly from behind. This radiation consists of isotropically emitted component connected with thermal gas and/or dust heated by the central source (the narrow line region and the dusty nuclear torus) plus an anisotropic blazar-like emission due to small scale highly relativistic nuclear jet. The narrow line emission and the radiation of dusty nuclear tours, typically weak or even absent in FR I radio galaxies (e.g., Chiaberge et al. 1999), are always negligible at distances  $r \geq 1$  kpc from the active nucleus (section 2.2.2, see also Celotti et al. 2001). Instead, as discussed below, comptonisation of starlight and extended dust emission of the host galaxy and, in some cases, comptonisation of the ‘hidden’ blazar radiation can dominate  $\gamma$ -ray output of the FR I large scale jets.

### 2.2.1. Synchrotron photons

For a simple evaluation of the synchrotron photons energy density in the jet comoving frame, we consider an approximately cylindrical knot region, with a radius  $R \leq 0.1$  kpc and a deprojected observed length  $l \sim R$ . In the case of a continuous jet one has  $l' = l\Gamma > R$ , and therefore

$$U'_{syn} = \frac{[\nu' L'_{\nu'}]_{syn,br}}{2\pi R l' c} = \frac{[\nu L_{\nu}]_{syn,br}}{2\pi R l c} \frac{1}{\delta^3} \sim 5.6 \cdot 10^{-11} \frac{[\nu L_{\nu}]_{syn,42}}{R_{-1}^2} \frac{1}{\delta^3} \text{ erg cm}^{-3} \quad , \quad (8)$$

where  $[\nu L_{\nu}]_{syn,42} \equiv [\nu L_{\nu}]_{syn,br}/10^{42} \text{ erg s}^{-1}$  and  $R_{-1} \equiv R/0.1 \text{ kpc}$ . If the emitting kpc-scale jet region is in fact a moving source, then  $l' = l/\delta = R/\delta$ , and the jet comoving energy density of the synchrotron emission is

$$U'_{syn} = \frac{[\nu' L'_{\nu'}]_{syn,br}}{2\pi R^2 c} = \frac{[\nu L_{\nu}]_{syn,br}}{2\pi R^2 c} \frac{1}{\delta^4} \sim 5.6 \cdot 10^{-11} \frac{[\nu L_{\nu}]_{syn,42}}{R_{-1}^2} \frac{1}{\delta^4} \text{ erg cm}^{-3} \quad . \quad (9)$$

The jet comoving synchrotron break frequency is  $\nu'_{syn,br} = \nu_{syn,br}/\delta$ . Note, that for the approximately constant  $\varphi \sim 0.1$ , the jet radius at a distance  $r \sim 1$  kpc from its base is expected to be  $R \sim 0.1$  kpc, consistently with the value considered here.



### 2.2.2. Radiation of the active nucleus

At first, let us consider the blazar-like (*bl*) emission of FR I active nuclei, which – according to the unification scheme (e.g., Urry and Padovani 1995) – belong to the low-luminous (BL Lac) blazar subclass. Due to relativistic effects, this radiation is strongly beamed into the cone with an opening angle  $\theta_{bl} \sim 1/\Gamma_{bl}$ , where  $\Gamma_{bl}$  is the nuclear jet bulk Lorentz factor. In order to evaluate energy density of this emission in the kpc-scale jet rest frame, we assume that it ‘enters’ into the considered emitting region directly from the jet base. In other words, we neglect any possible misalignment between the pc-scale and the kpc-scale jets. The respective energy density of the blazar photons is then

$$U'_{bl} \sim \frac{L_{bl}(0)}{4\pi r^2 c} \frac{1}{(2\Gamma)^2} \quad , \quad (10)$$

where  $L_{bl}(0)$  is the isotropic luminosity of the blazar emission evaluated by the stationary observer located at  $\theta = 0$  (Appendix B). With the spatial scales of the kpc-scale jet emitting region much larger than the characteristic nuclear scales ( $R, r \gg r_0$ ), the discussed source of the seed photons for the inverse-Compton scattering should be considered as a *stationary* one. A typical short time scale of blazar variability justifies this statement. Therefore,

$$L_{bl}(0) = L_{bl} \frac{\delta_{bl, \theta=0}^3 / \Gamma_{bl}}{\delta_{bl}^3 / \Gamma_{bl}} \sim L_{bl} \left( \frac{2\Gamma_{bl}}{\delta_{bl}} \right)^3 \quad , \quad (11)$$

where  $\delta_{bl} = [\Gamma_{bl} (1 - \beta_{bl} \cos \theta)]^{-1}$  and  $L_{bl}$  is the isotropic luminosity of the considered stationary blazar source measured by the observer located at the angle  $\theta$  to the jet axis. Hence,

$$U'_{bl} \sim \frac{L_{bl} \Gamma_{bl}^3}{2\pi r^2 c \delta_{bl}^3} \frac{1}{\Gamma^2} \sim 5.6 \cdot 10^{-13} \frac{L_{bl,42} \Gamma_{bl}^3}{r_1^2 \delta_{bl}^3} \frac{1}{\Gamma^2} \quad \text{erg cm}^{-3} \quad , \quad (12)$$

where we put  $L_{bl,42} \equiv L_{bl}/10^{42} \text{ erg s}^{-1}$  (cf. equation 1 in Celotti et al. 2001).

Typically, for the high energy peaked BL Lacs (HBLs) the observed synchrotron luminosity is  $10^{44} - 10^{46} \text{ erg s}^{-1}$ , while for the low energy peaked BL Lacs (LBLs) it is in the range  $10^{45} - 10^{47} \text{ erg s}^{-1}$  (Fossati et al. 1998). An another subclass of blazar sources – the flat spectrum radio quasars (FSRQs) – have even higher observed luminosities. However, in a framework of the unification scheme FSRQs correspond to the FR II sources. The critical observed synchrotron frequency of blazar emission, which anticorrelates with the blazar synchrotron luminosity, is usually  $10^{15} - 10^{17} \text{ Hz}$  for HBLs and  $10^{13} - 10^{15} \text{ Hz}$  for LBLs (again Fossati et al. 1998). Below, we take  $L_{bl} \sim [\nu L_\nu]_{bl, br}$ , where the blazar synchrotron break frequency in the jet comoving frame is  $\nu'_{bl, br} \sim \nu_{bl, br}(0)/\Gamma$ , and  $\nu_{bl, br}(0) = \nu_{bl, br} (2\Gamma_{bl}/\delta_{bl})$ . We also assume, that the blazar source illuminates uniformly the whole kpc-scale jet emitting

region. Note, that for the typical  $\Gamma_{bl} \sim 10$ , the half-angle of the blazar emission cone is equal to the assumed jet opening angle,  $\theta_{bl} \sim \varphi \sim 0.1$ .

As mentioned previously, the isotropic component of the nuclear (*nucl*) emission, i.e. radiation of narrow line region or dusty nuclear torus, are weak or even absent in FR I radio galaxies (isotropic luminosity  $L_{nucl} < 10^{42}$  erg/s). For the observer located at the distance  $r$  from the active center and moving with the Lorentz factor  $\Gamma$  along the jet axis, energy density of the considered circumnuclear isotropic emission scales in the same manner as the energy density of the blazar radiation – in both cases the appropriate relations are  $U'_{nucl} \sim L_{nucl}/4\pi r^2 c(2\Gamma)^2$  and the one given in equation 10, respectively. Therefore, as  $L_{nucl} \ll L_{bl}(0)$ , the isotropically emitted nuclear photon fields are negligible as compared to the blazar emission.

### 2.2.3. CMB and galactic photon fields

AGNs are hosted by elliptical galaxies, whose extended optical and infrared emission contribute significantly to the total radiation intensity at the kiloparsec distances from the galactic centers.

Ellipticals are known to contain  $\sim 1 M_{\odot}$  stars evolving from the main sequence through the red-giant phase, hot interstellar gas heated to temperatures  $\sim 10^7$  K and radiating at X-rays, and, finally, dust prominent at infrared frequencies. Photospheric emission from cool giant stars, which are concentrated within a few hundreds of parsecs from the galactic center (i.e. within a ‘central bulge’ or a ‘galactic core’), dominates bolometric luminosities of the discussed galaxies and peaks in the range  $\sim 1 - 3 \mu\text{m}$  (e.g., Knapp et al. 1992). Total bolometric luminosities of giant ellipticals can be as high as  $\sim 3 \cdot 10^{11} L_{\odot} \sim 10^{45}$  erg/s. Emission at wavelengths  $5 - 20 \mu\text{m}$  is analogously distributed as the starlight and is most likely connected with dusty winds accompanying the red-giant stars and forming their dusty circumstellar envelopes (Knapp et al. 1992; Tsai and Mathews 1995). Radio galaxies are in general more luminous at infrared wavelengths as compared to the normal ellipticals (by a factor of 2 – 3 relative to the starlight emission), with  $\sim 10 \mu\text{m}$  luminosity being on average two orders of magnitude lower than the bolometric one (Knapp et al. 1990). In addition to the circumstellar dust emission, ellipticals exhibit also an excess at far-infrared frequencies, peaking around  $60 - 100 \mu\text{m}$ . If the cold dust responsible for production of these photons is optically thin, it must occupy regions that extend far from the galactic core (a few times the core radius), in order to avoid overheating by the starlight (Tsai and Mathews 1996). An alternative explanation can be provided by concentration of the cold dust in disks and lanes self-shielded from the starlight and located closer to the galactic center. The far-infrared

excess is especially prominent in radio galaxies (Golombek et al. 1988; Knapp et al. 1990). However, as the origin and spatial distribution of this radiation is unknown, and also as the far-infrared emission shows significant variations from galaxy to galaxy, we do not discuss its contribution to the kpc-scale jet inverse-Compton emission.

In Appendix C, following Tsai and Mathews (1995), we estimate the energy density of the starlight (*star*) photons to be  $U_{star} \sim 10^{-9}$  erg/cm<sup>3</sup> at the distance  $\sim 1$  kpc from the center of the typical giant elliptical galaxy. Assuming for simplicity an approximately isotropic distribution of the stellar emission at this scale, in the jet comoving frame one has

$$U'_{star} \sim U_{star} \Gamma^2 \sim 10^{-9} \Gamma^2 \text{ erg cm}^{-3} \quad (13)$$

(Appendix B), with a characteristic starlight frequency  $\nu'_{star} \sim 10^{14} \Gamma$  Hz. The galactic dust emission (*dust*) is distributed analogously to the stellar radiation and hence its energy density in the jet rest frame is also amplified approximately by a factor  $\Gamma^2$ . In this paper we take

$$U'_{dust} \sim 0.01 \cdot U'_{star} \sim 10^{-11} \Gamma^2 \text{ erg cm}^{-3} \quad (14)$$

at  $\nu'_{dust} \sim 3 \cdot 10^{13} \Gamma$  Hz. Finally, for redshifts  $z \ll 1$  an analogous energy density of the blackbody CMB is equal to

$$U'_{CMB} = a T_{CMB}^4 \Gamma^2 \sim 4 \cdot 10^{-13} \Gamma^2 \text{ erg cm}^{-3} \quad , \quad (15)$$

where  $a = 7.53 \cdot 10^{-15}$  cgs and the observed CMB temperature is  $T_{CMB} = 2.7$  K. The appropriate characteristic CMB photon frequency is  $\nu'_{CMB} \sim 2 \cdot 10^{11} \Gamma$  Hz.

### 2.3. Inverse-Compton emission: $\gamma$ -rays

With the evaluated photon fields in the emitting region rest frame,  $U'_{seed}$ , one can estimate the observed break luminosity of the appropriate inverse-Compton (*ic(seed)*) emission in the Thomson regime as

$$[\nu L_\nu]_{ic(seed),br} \sim f_{\pm/iso}(\Gamma, \theta) \frac{U'_{seed}}{U'_B} [\nu L_\nu]_{syn,br} \quad . \quad (16)$$

Presence of an additional factor  $f_{\pm/iso}(\Gamma, \theta)$  is connected with the possible anisotropy of the external radiation fields within the jet comoving frame, in cases of its relativistic bulk velocities and/or non-isotropic photon distribution in the galaxy rest frame. As shown in Appendix D,

$$f_{\pm/iso}(\Gamma, \theta) = \begin{cases} \frac{3}{4} (\delta/\Gamma)^2 [(1 + \mu)/(1 + \beta)]^2 & (+) \\ \frac{3}{4} (\delta \Gamma)^2 [(1 - \mu)(1 + \beta)]^2 & (-) \\ 1 & (iso) \end{cases} \quad (17)$$

respectively for the cases when the seed photons are distributed isotropically in the galaxy rest frame near the kpc-scale jet (+), when they illuminate the jet exactly from behind (–), or when they are isotropic *in* the jet comoving frame (*iso*). Luminosity  $[\nu L_\nu]_{ic(seed),br}$  is related to the observed flux of the inverse-Compton emission,  $[\nu S_\nu]_{ic(seed),br}$ , by the relation

$$[\nu S_\nu]_{ic(seed),br} = \frac{[\nu L_\nu]_{ic(seed),br}}{4\pi D^2} \quad , \quad (18)$$

where  $D$  is a distance to the source. The appropriate observed inverse-Compton break frequency due to  $\gamma_{br}$  electrons scattering the seed photons with the observed characteristic (break) frequency  $\nu_{seed}$  is

$$\nu_{ic(seed),br} = h_{\pm/iso}(\Gamma, \theta) \gamma_{br}^2 \nu_{seed} \quad , \quad (19)$$

where

$$h_{\pm/iso}(\Gamma, \theta) = \begin{cases} \delta^2 (1 + \mu)/(1 + \beta) & (+) \\ \delta^2 (1 - \mu) (1 + \beta) & (-) \\ 4/3 & (iso) \end{cases} \quad (20)$$

(Appendix E). Assuming that the scattering proceeds in the Thomson regime,

$$\gamma_{br} \nu'_{seed} < \frac{mc^2}{h} \quad , \quad (21)$$

the inverse-Compton spectrum for  $\nu_{ic(seed)} < \nu_{ic(seed),br}$  is a power-law with a spectral index corresponding to the radio-to-optical synchrotron continuum,  $\alpha_\gamma \sim (p - 1)/2$  (equation 1), while for  $\nu_{ic(seed)} > \nu_{ic(seed),br}$  it is expected to steepen by  $\Delta\alpha$ . The high energy cut-off in the observed  $\gamma$ -ray emission can result from the cut-off in the electron energy distribution ( $\gamma_{max}$ ), from entering the Klein-Nishina (KN) regime or due to external absorption on the CIB radiation.

Below, we evaluate fluxes and break energies of the inverse-Compton emission on photon fields described in the previous section. At first we discuss the synchrotron self-Compton radiation, i.e. the inverse-Compton scattering of the synchrotron photons produced by the same electron population (*ic = ssc; seed = syn*). Next, we analyse the external-Compton (*ic ≡ ec*) process starting from comptonisation of the ‘hidden’ blazar emission (*seed = bl*). Then we discuss the scattering of CMB photons and different radiation fields of the host galaxy (*seed = star, dust, CMB*).

### 2.3.1. Synchrotron self-Compton emission

From the equations 8 - 9 and 16 - 18 with  $f_{iso}(\Gamma, \theta) = 1$ , one obtains the observed SSC energy flux for the two considered cases of a continuous jet and a moving blob

$$[\nu S_\nu]_{ssc, br} \sim 1.2 \cdot 10^{-11} \frac{[\nu L_\nu]_{syn, 42}^2}{B_{-4}^2 R_{-1}^2 D_{10}^2} \begin{cases} \delta^{-3} & (cj) \\ \delta^{-4} & (mb) \end{cases} \frac{\text{erg}}{\text{s cm}^2} \quad (22)$$

respectively, where  $D_{10} \equiv D/10$  Mpc. Equations 19 - 20 with  $h_{iso}(\Gamma, \theta) = 1$  give the observed SSC break energy

$$\varepsilon_{ssc, br} \sim 1.5 \cdot 10^{11} \frac{\nu_{syn, 14}^2}{B_{-4}} \frac{1}{\delta} \text{ eV} \quad . \quad (23)$$

The Thomson regime condition for the discussed process reads as

$$\nu_{syn, 14} < 2 B_{-4}^{1/3} \delta \quad . \quad (24)$$

The SSC emission is determined by the observed parameters  $[\nu L_\nu]_{syn, br}$  and  $\nu_{syn, br}$ , plus the emitting region linear size  $R$ , the (unknown) magnetic field  $B$  and the kinematic factor  $\delta$ . Typically, for the FR I *Chandra* jets one has  $[\nu L_\nu]_{syn, 42} < 1$ ,  $R_{-1} \sim 1$  and the equipartition value (as computed for nonrelativistic bulk velocities)  $B_{-4} \sim 1$ . Hence, for  $\nu_{syn, 14} \sim 1$  and the usually considered  $\delta \sim 1$ , one can put an upper limit  $[\nu S_\nu]_{ssc, br} < 10^{-11} D_{10}^{-2} \text{ erg/s cm}^2$  at the critical photon energy  $\varepsilon_{ssc, br} \sim 0.1$  TeV. Future *IACT* systems will be able to eventually detect such emission<sup>5</sup> from the sources at the distances  $D < 100$  Mpc. Higher SSC flux than discussed above can be produced for a given  $[\nu L_\nu]_{syn, br}$  in the case of a strong departure from the equipartition,  $B \ll B_{eq}$ , and/or for a de-beaming of the jet emission,  $\delta \ll 1$ . However, for decreasing  $B$  and  $\delta$  the effects connected with the KN regime are expected to become important (unless  $\nu_{syn, 14} \ll 1$ , equation 24), decreasing the efficiency of the SSC process.

### 2.3.2. Comptonisation of the hidden blazar emission

From the equations 12 and 16 - 20, one obtains the observed EC(bl) energy flux

$$[\nu S_\nu]_{ec(bl), br} \sim 1.2 \cdot 10^{-13} \frac{[\nu L_\nu]_{bl, 42} [\nu L_\nu]_{syn, 42} \Gamma_{bl}^3 f_-}{B_{-4}^2 r_1^2 D_{10}^2 \delta_{bl}^3} \frac{f_-}{\Gamma^2} \frac{\text{erg}}{\text{s cm}^2} \quad , \quad (25)$$

---

<sup>5</sup>with the detector sensitivity  $\geq 10^{-13} \text{ erg/s cm}^2$  for  $5\sigma$  detection threshold and 100 h observation (Aharonian 1998)

and the observed EC(bl) break energy

$$\varepsilon_{ec(bl),br} \sim 2.2 \cdot 10^{11} \frac{\nu_{bl,14} \nu_{syn,14} \Gamma_{bl}}{B_{-4} \delta_{bl}} \frac{h_-}{\delta} \text{ eV} \quad . \quad (26)$$

The Thomson regime condition for the considered process reads as

$$\Gamma_{bl} \delta_{bl}^{-1} \nu_{bl,14} < \Gamma \delta^{1/2} B_{-4}^{1/2} \nu_{syn,14}^{-1/2} \quad . \quad (27)$$

The EC(bl) emission is determined by the jet parameters  $[\nu L_\nu]_{syn,br}$  and  $\nu_{syn,br}$  plus the distance from the blazar source  $r$ , the unknown magnetic field  $B$ , kinematic factors  $\Gamma$  and  $\theta$  and, finally, by properties of the blazar core  $[\nu L_\nu]_{bl,br}$ ,  $\nu_{bl,br}$  and  $\Gamma_{bl}$ . For the usually discussed  $\delta \sim 1$  and  $\theta \geq 45^\circ$ , typical  $\nu_{syn,14} \sim 1$  and the equipartition value  $B_{-4} \sim 1$ , one expects the observed EC(bl) break energy to be  $\varepsilon_{ec(HBL),br} \sim 1 - 100$  TeV in the case of comptonisation of HBL radiation ( $bl \equiv HBL$ ), and  $\varepsilon_{ec(LBL),br} \sim 0.01 - 1$  TeV in the case of LBL-like core emission ( $bl \equiv LBL$ ). As the synchrotron break frequency of the blazar emission is anticorrelated with the blazar synchrotron luminosity (see section 2.2.2), one can put upper limits on the observed EC(bl) fluxes  $[\nu S_\nu]_{ec(HBL),br} < 10^{-11} D_{10}^{-2} \text{ erg/s cm}^2$  for  $\varepsilon_{ec(HBL),br} \sim 1$  TeV (taking a rough estimate  $L_{HBL,max}(0) \leq 10^{46} \text{ erg/s}$ ), and  $[\nu S_\nu]_{ec(LBL),br} < 10^{-10} D_{10}^{-2} \text{ erg/s cm}^2$  for  $\varepsilon_{ec(LBL),br} \sim 10$  GeV (with  $L_{LBL,max}(0) \leq 10^{47} \text{ erg/s}$ ). In addition, the EC(HBL) emission is expected to be significantly decreased due to the KN effects, contrary to the EC(LBL) radiation. For the discussed standard jet parameters the latter one could be observed by *GLAST*<sup>6</sup> from sources with  $D < 100$  Mpc. Similarly to the case of the SSC process, for a given  $[\nu L_\nu]_{syn,br}$  the subequipartition magnetic field and/or large jet inclination increase the expected value of  $[\nu S_\nu]_{ec(bl),br}$ .

### 2.3.3. Comptonisation of the galactic photon fields and CMB radiation

From the equations 13 and 16 - 20, one obtains the observed EC(star) energy flux

$$[\nu S_\nu]_{ec(star),br} \sim 2.1 \cdot 10^{-10} \frac{[\nu L_\nu]_{syn,42}}{B_{-4}^2 D_{10}^2} f_+ \Gamma^2 \frac{\text{erg}}{\text{s cm}^2} \quad , \quad (28)$$

and the observed EC(star) break energy

$$\varepsilon_{ec(star),br} \sim 1.1 \cdot 10^{11} \frac{\nu_{syn,14}}{B_{-4}} \frac{h_+}{\delta} \text{ eV} \quad . \quad (29)$$

---

<sup>6</sup>accordingly to the 10 GeV *GLAST* sensitivity  $\sim 10^{-12} \text{ erg/s cm}^2$  for  $5\sigma$  detection threshold in 1 year all-sky survey (Aharonian 1998)

The considered process proceeds within the Thomson regime for

$$\nu_{syn,14} < 6 B_{-4} \frac{\delta}{\Gamma^2} . \quad (30)$$

The EC(star) radiation is determined by the jet parameters  $[\nu L_\nu]_{syn,br}$ ,  $\nu_{syn,br}$ ,  $B$  and  $\delta$ , as well as by properties of the host galaxy ( $L_{star}$ , etc). For non-relativistic jets, typical  $\nu_{syn,14} \sim 1$ ,  $[\nu L_\nu]_{syn,42} < 1$  and  $B_{-4} \sim 1$ , the break energy of the considered emission is  $\varepsilon_{ec(star),br} \sim 0.1$  TeV, and the observed energy flux is  $[\nu S_\nu]_{ec(star),br} < 10^{-10} D_{10}^{-2}$  erg/s cm<sup>2</sup>. However, this relatively strong radiation can be significantly decreased in the case of relativistic jet velocities and large jet inclinations to the line of sight due to both the KN and the Doppler effects (equations 30 and 28, respectively). The eventual Doppler-hide results from the beaming pattern of the EC(star) emission, which – contrary to the discussed before SSC and EC(bl) processes – is maximised for small jet viewing angles (for a given  $[\nu L_\nu]_{syn,br}$  one has  $[\nu S_\nu]_{ec(star),br} \propto f_+ \Gamma^2 \sim \delta^2$ ; equation 28). Comptonisation of the galactic infrared emission, as well as of the CMB radiation, is not expected to suffer such a decrease connected with the KN regime. For example, the Thomson regime condition for the EC(dust) process can be rewritten as  $\nu_{syn,14} < 60 B_{-4} \delta \Gamma^{-2}$ . For the standard nonrelativistic jet parameters, one can therefore put an upper limit  $[\nu S_\nu]_{ec(dust),br} < 10^{-12} D_{10}^{-2}$  erg/s cm<sup>2</sup> at  $\varepsilon_{ec(dust),br} \geq 10$  GeV. At even lower photon energies the EC(CMB) emission dominates, proceeding well in the Thomson regime, with the maximum placed near  $\varepsilon_{ec(CMB),br} \sim 0.1$  GeV. The observed flux of this radiation is relatively low,  $[\nu S_\nu]_{ec(CMB),br} < 10^{-13} D_{10}^{-2}$  erg/s cm<sup>2</sup>. Detection of this emission from the FR I jets located further than a few Mpc (i.e. further than Centaurus A) by future  $\gamma$ -ray telescopes is therefore possible only if the jet Doppler factor is significantly larger than unity, and/or if  $B \ll B_{eq}$ . On the other hand, large values of  $\delta$  are unlikely to occur in the FR I jets, although, as mentioned in section 2.1, the optical and X-ray jets can constitute the exceptions from this picture.

### 3. Centaurus A and M 87

The resulting inverse-Compton fluxes and break energies evaluated in the previous section depend on several free parameters. Because of relatively wide range of values covered by them, it is difficult to discuss  $\gamma$ -ray emission of the considered objects in general. Instead, a detailed analysis can be performed for each individual source. In this section, we discuss the large scale jet  $\gamma$ -ray radiative outputs of Centaurus A and M 87. One may note at this point, that both sources are quite unique. They are relatively nearby, what allowed in the past to study their jets at different frequencies and scales, with high spatial and spectral resolutions. The large scale jet in M 87 is the first one discovered at optical frequencies.

Both sources were among a few radio-loud AGNs known to possess the large scale X-ray jets before *Chandra* was launched. During the last decades, M 87 and Centaurus A were also being frequently observed at  $\gamma$ -rays, from sub-MeV to TeV photon energies, what resulted in positive detections or constraints on the flux upper limits.

### 3.1. Centaurus A

Centaurus A galaxy is a giant elliptical, which most probably merged in the past with an other small and gas rich galaxy. With the distance  $D = 3.5$  Mpc Centaurus A hosts the closest AGN, which is however difficult to be observed at IR and optical frequencies because of the obscuring dust lane. VLA studies (e.g., Burns et al. 1983; Clarke et al. 1992) show a double-lobed morphology of the Centaurus A radio source, with the jet and the counterjet of the FR I type and a kinetic power  $\sim 2 \cdot 10^{43}$  erg/s. VLBI observations (e.g., Jones et al. 1996) followed the jet and the counterjet to the pc-scales, suggesting the jet viewing angle  $\theta \sim 50^\circ - 80^\circ$ . Optical and IR observations of the Centaurus A nucleus (e.g., Bailey et al. 1986; Hawarden et al. 1993; Packham et al. 1996; Schreier et al. 1996, 1998; Marconi et al. 2000; Capetti et al. 2000) revealed the unresolved ( $< 1$  pc) and variable central source with a small ( $\sim 40$  pc) nuclear disc and a possible extremely compact nuclear torus. No IR/optical emission connected directly with the jet non-thermal radiation was found (but see Joy et al. 1991; Schreier et al. 1996, 1998; Marconi et al. 2000). At the X-rays, the jet was observed in addition to the variable (at the time scales from minutes up to years) nuclear component (Schreier et al. 1979; Morini et al. 1989, respectively). Recently, *Chandra* telescope revealed details of the jet X-ray emission and presence of the X-ray counterjet (Kraft et al. 2002; Hardcastle et al. 2003), as well as of the whole Centaurus A system (Karovska et al. 2002). At higher energies, Centaurus A was observed by *CGRO* satellite, what allowed to detect the maximum of its nuclear  $\gamma$ -ray emission near  $\sim 0.1$  MeV (Steinle et al. 1998). For  $\varepsilon_\gamma > 0.1$  MeV the  $\gamma$ -ray flux decreases, although at  $\sim 100$  MeV photon energies it is still detectable (Sreekumar et al. 1999). *CANGAROO* observations of the extended ( $\sim 14$  kpc) region around Centaurus A nucleus put the upper limit on the emission at the VHE range,  $S(\varepsilon_\gamma \geq 1.5 \text{ TeV}) < 1.28 \cdot 10^{-11} \text{ ph cm}^{-2} \text{ s}^{-1}$  (Rowell et al. 1999). However, the discussed object was detected in the past at TeV energies, with the observed flux  $S(\varepsilon_\gamma \geq 0.3 \text{ TeV}) \sim 4.4 \cdot 10^{-11} \text{ ph cm}^{-2} \text{ s}^{-1}$  (Grindlay et al. 1997), what made Centaurus A the very first (although not confirmed) detected extragalactic source of the VHE radiation. Recent upper limit suggests that this emission can be variable on a timescale of years, in analogy to the low- and high-states of activity known from the TeV blazar observations (but see also Harris et al. 1997, 2003, for the X-ray variability of the large scale jet emission in M 87).



Existence of a hidden BL Lac core in the Centaurus A nucleus, as expected in a framework of unification scheme, was widely discussed over the last decade (Bailey et al. 1986; Morganti et al. 1991; Hawarden et al. 1993; Packham et al. 1996; Steinle et al. 1998; Capetti et al. 2000). Most recently, Chiaberge et al. (2001) reconstructed broad-band spectrum of Centaurus A nucleus, from radio to  $\gamma$ -ray frequencies, and found spectacular similarities to the characteristic double-peaked blazar spectral energy distribution. The synchrotron component of this radiation was found to peak at far infra-red energy range,  $\nu_{bl,br} \sim 10^{12} - 10^{13}$  Hz, with the observed luminosity  $[\nu L_\nu]_{bl,br} \sim 10^{41} - 10^{42}$  erg/s. The inverse-Compton break energy was placed near  $\sim 0.1$  MeV, with the observed power comparable to the synchrotron one. Chiaberge et al. fitted the SSC model to the multiwavelength Centaurus A nucleus emission, and found that all (except one) intrinsic parameters are similar to those of the low-luminous blazar sources. The only difference, as compared to the ‘typical’ BL Lac broad-band spectrum, was a small value of the required Doppler factor,  $\delta_{bl} \sim 1.6$ . Chiaberge et al. interpreted their results as the evidence for the jet radial velocity structure at pc-scales, consisting of a fast central spine surrounded by a slower boundary layer (see also Chiaberge et al. 2000). Assuming that the physical properties (i.e. electron energy distribution, magnetic field intensity, etc) are the same in both jet components, the observed multiwavelength spectrum of the Centaurus A nucleus can then be regarded as a representation of a typical low-luminous blazar emission, but originating within the slower jet boundary layer and therefore less beamed as compared to the ‘classical’ BL Lacs. It is consistent with the jet inclination  $\sim 70^\circ$ . Most probably, Centaurus A observed at small angles to the jet axis would be therefore classified as LBL, with the observed luminosity  $\sim 10^{45} - 10^{46}$  erg/s and with the observed break frequency  $\sim 10^{13} - 10^{14}$  Hz. Note, that in such a case the Centaurus A nucleus is not expected to radiate at the VHE range (cf. Bai and Lee 2001). For the estimates below, we assume  $[\nu L_\nu]_{bl,42} \sim 0.3$ ,  $\nu_{bl,14} \sim 0.01$ ,  $\Gamma_{bl} \sim 10$  and  $\delta_{bl} \sim 1.6$ .

In order to discuss the  $\gamma$ -ray emission of the large scale jet in Centaurus A, let us consider its brightest part in X-rays and at radio frequencies, the ensemble of the knots A1 - A4. The X-ray observations (Kraft et al. 2002) suggest that for this region  $R_{-1} \sim 0.8$ ,  $r_1 \sim 0.4$ ,  $B_{-4} \sim 0.6$ ,  $\alpha_X \sim 1.5$  and  $L_X \sim 4 \cdot 10^{39}$  erg/s. The synchrotron break frequency is unknown, as there is no observation of the jet synchrotron emission at IR/optical frequencies. However, the existing upper limits (Schreier et al. 1996) are consistent with the synchrotron spectrum resulting from the electron energy distribution given by equation 1, with  $\alpha_R \sim 0.5$ ,  $\Delta\alpha \sim 1$  and the assumed  $\nu_{syn,14} \sim 1$ . Thus, below we put  $[\nu L_\nu]_{syn,br}/L_X \sim (10^{14} \text{ Hz}/2.4 \cdot 10^{17} \text{ Hz})^{1-\alpha_X}$ , implying for the A1 - A4 region  $[\nu L_\nu]_{syn,42} \sim 0.2$ . Below we also take the galactic photons energy densities  $U_{star}$  and  $U_{dust}$  as estimated in section 2.2.3<sup>7</sup>.

---

<sup>7</sup>12  $\mu\text{m}$  flux from Centaurus A is 23 Jy (Knapp et al. 1990).

For the considered parameters of Centaurus A, the IC fluxes and break energies in function of the jet viewing angle  $\theta$  are presented on Figure 1, for two different jet bulk Lorentz factors  $\Gamma = 2, 6$ . For small values of  $\theta$  the EC(star) and EC(dust) emissions dominate, while for large jet inclinations the SSC and the EC(bl) processes are the more important ones. In general, small jet viewing angles are excluded as they imply non-observed large VHE flux due to comptonisation of the starlight. However, for large jet inclinations the SSC radiation also seems to overproduce (comparing to the present upper limits) the VHE photons. For example, for the usually considered  $\theta = 70^\circ$  and  $\Gamma \leq 2$ , the expected SSC energy flux is  $[\nu S_\nu]_{ssc,br} \sim 10^{-10} \text{ erg s}^{-1} \text{ cm}^{-2}$  at the observed break energy  $\varepsilon_{ssc,br} \sim 0.1 - 1 \text{ TeV}$ . This suggest presence of the KN effects decreasing the SSC and the EC(star) emissions, what in turn indirectly suggests relativistic jet velocities ( $\Gamma > 2$ , Figure 2) and/or subequipartition magnetic field ( $B \leq 10^{-5} \text{ G}$ , Figure 3). Alternatively, the unobserved synchrotron break frequency  $\nu_{syn,br}$  can be higher than assumed here  $10^{14} \text{ Hz}$ .

For the moderate and large jet inclinations, the EC(bl) radiation is expected to be very strong, with the observed flux  $[\nu S_\nu]_{ec(bl),br} \sim 10^{-11} - 10^{-10} \text{ erg s}^{-1} \text{ cm}^{-2}$  and  $\varepsilon_{ec(bl),br} \sim 10 \text{ GeV}$  (for  $\Gamma = 1 - 10$ ). This emission could be therefore easily observed in the future by the *GLAST* satellite. The EC(dust) emission is important only for  $\delta \gg 1$ , and otherwise is dominated by the EC(bl) radiation. Finally, comptonisation of the CMB radiation does not play a role in the  $\gamma$ -ray emission of Centaurus A unless  $\delta \gg 1$  or  $B \ll B_{eq}$  (Figures 1 and 3).

### 3.2. M 87

M 87 galaxy is a giant elliptical, placed in the center of the Virgo Cluster X-ray emission. With the distance  $D = 16 \text{ Mpc}$  it hosts one of the closest AGNs, with spectacular and widely studied large scale structure. VLA observations of the M 87 radio source revealed one-sided, highly polarised and edge-brightened radio jet (e.g., Owen et al. 1989), in addition to the large scale cavities inflated in the intergalactic medium (Owen et al. 2000). A relatively high radio luminosity places the discussed object at the borderline between FR I and FR II radio sources, although the one-sided jet with a kinetic power  $\sim 5 \cdot 10^{44} \text{ erg/s}$  displays FR I morphology. Detailed VLA and HST studies (Biretta et al. 1995, 1999, respectively) revealed apparent superluminal motions of the jet components at distances up to a few hundreds parsecs from the active center, while VLBI observations measured much lower velocities at parsec scales. This suggests a complex velocity structure of the M 87 jet, with highly relativistic bulk velocities over all of its length ( $\Gamma \sim \text{a few}$ ) and a relatively small jet inclination to the line of sight ( $\theta \sim 30^\circ$ ; e.g., Bicknell and Begelman 1996). IR observations

of the considered object (Whysong and Antonucci 2001; Corbin et al. 2002) give no evidence for the presence of an obscuring matter around the active center as expected for AGNs, consistently with a lack of the dusty nuclear torus or, eventually, with its small size ( $< 50$  pc). Optical observations of the M 87 nuclear region revealed a small disc ( $\sim 100$  pc) of ionised gas with a LINER emission line spectrum, fuelling a supermassive central black hole (e.g., Macchetto et al. 1997). The optical nuclear emission presents a smooth featureless continuum variable at time scales of months and connected with an unresolved ( $\leq 5$  pc) central source (Tsvetanov et al. 1998). The large scale jet is very prominent and highly polarised in optical, what allows to perform its detailed radio-to-optical spectroscopy and polarimetry (e.g., Meisenheimer et al. 1996; Sparks et al. 1996; Perlman et al. 1999, 2001). At X-rays the jet and the nucleus were early observed by *ROSAT* satellite (e.g., Schreier et al. 1982). These observations allowed to construct broad-band radio-to-X-ray spectrum of the large scale jet emission (e.g., Biretta et al. 1991), to put constraints on the X-ray nuclear radiation and its variability (Harris et al. 1997) and, finally, to study interaction between the radio-emitting matter and the surrounding thermal gas within the extended M 87 halo (Böhringer et al. 1995, 2001). Recently, the X-ray jet radiation was studied in more detail by *Chandra* (Marshall et al. 2002; Wilson and Yang 2002; Harris et al. 2003). Besides several attempts in the past, till the last year M 87 was not detected in  $\gamma$ -rays, neither by *CGRO* satellite (Sreekumar et al. 1996) nor by ground-based detectors in the VHE range. Up to now, the existing upper limit on the TeV emission of the discussed object was  $S(\varepsilon_\gamma \geq 0.21 \text{ TeV}) < 1.2 \cdot 10^{-10} \text{ ph cm}^{-2} \text{ s}^{-1}$  (Weekes et al. 1972). However, recent *HEGRA* observations resulted in positive detection of the VHE emission from the M 87 radio galaxy, with the observed flux  $S(\varepsilon_\gamma \geq 0.73 \text{ TeV}) \sim 0.96 \cdot 10^{-12} \text{ ph cm}^{-2} \text{ s}^{-1}$  (Aharonian et al. 2003).

Similarly to the case of Centaurus A, presence of a hidden blazar in the nucleus of M 87 was discussed previously by, e.g., Tsvetanov et al. (1998); Reynolds et al. (1999); Whysong and Antonucci (2001); Corbin et al. (2002). However, contrary to Centaurus A, a broad-band spectrum of the discussed central source in the IR-to-UV frequencies – and therefore parameters of the considered hidden blazar – is poorly constrained. One may note, that the radio-to-X-ray nuclear radiation is roughly similar to the large scale jet synchrotron emission, with  $\alpha_{RO} < 1$  and  $\alpha_{OX} > 1$  (Tsvetanov et al. 1998; Böhringer et al. 2001). This indicates, that the nuclear radio-to-X-ray continuum possibly results from the synchrotron emission of one electron population, as expected for the low-luminous blazars, with the observed synchrotron spectral break  $\nu_{bl,br}$  placed near optical frequencies. The observed synchrotron power is then  $\sim 3 \cdot 10^{42} \text{ erg/s}$  (Tsvetanov et al. 1998). Furthermore, one may assume that, in analogy to Centaurus A, the observed M 87 blazar-like emission originates from a slower component of the blazar jet and, hence, that the Doppler factor of the discussed radiation

is close to unity. Here we take  $\nu_{bl,14} \sim 10$  and  $[\nu L_\nu]_{bl,42} \sim 1$  with the assumed  $\Gamma_{bl} \sim 10$  and  $\delta_{bl} \sim 2$ . The above values suggest that the considered M 87 blazar is situated on the borderline between LBL and HBL subclasses, and only large jet inclination preclude us to observe its ‘classical’ blazar properties (cf. Bai and Lee 2001).

In order to evaluate the  $\gamma$ -ray flux of the M 87 large scale jet, let us consider its brightest knot A, dominating radio-to-X-ray radiative jet output. Besides differences in the jet morphology as observed in different frequencies, multiwavelength studies (e.g., Biretta et al. 1991; Meisenheimer et al. 1996; Perlman et al. 2001; Marshall et al. 2002; Wilson and Yang 2002) allow one to construct broad-band spectrum of the considered region. They indicate  $R_{-1} \sim 0.8$  (at radio and optical; X-ray knots seem to be twice narrower),  $r_1 \sim 1$ ,  $B_{-4} \sim 2.5$  and the synchrotron power  $\sim 10^{42}$  erg/s. The exact value of the spectral break (and hence of the synchrotron break luminosity) depends on the detailed model of the synchrotron emission assumed for the knot regions (Perlman et al. 2001; Marshall et al. 2002). However, the average optical spectral index  $\alpha_O \sim 0.9$  (Perlman et al. 2001) indicates that  $\nu_{syn,br}$  is higher than  $10^{14}$  Hz. Below, for a rough estimate, we put  $\nu_{syn,14} \sim 10$  and  $[\nu L_\nu]_{syn,42} \sim 0.3$  (Wilson and Yang 2002). We also take the galactic photons energy densities  $U_{star}$  and  $U_{dust}$  as estimated in section 2.2.3<sup>8</sup>.

A similar analysis as for the Centaurus A  $\gamma$ -ray emission suggests, that in the case of M 87 large scale jet the EC(star) and EC(dust) processes should dominate production of the VHE photons (Figure 4). If the TeV flux detected recently by Aharonian et al. (2003) is in fact due to the knot A inverse-Compton emission, its most likely origin is comptonisation of the galactic stellar and circumstellar dust radiation. However, because of the expected KN effects, a detailed numerical analysis is required in order to find constraints on the jet bulk Lorentz factor and the magnetic field (cf. Figures 5 and 6). Possibilities that  $\delta > 1$  and  $B < B_{eq}$  could be additionally verified by the eventual detection of the EC(CMB) emission (Figures 4 and 6). The other IC processes for the M 87 jet are expected to be negligible because of the KN effects.

#### 4. Discussion and Conclusions

In this paper we discussed the high energy  $\gamma$ -ray emission of the FR I large scale jets. We used the X-ray observations compiled with data from the other spectral bands in order to reconstruct energy distribution of ultrarelativistic electrons present in the considered objects. Our phenomenological approach to recover electron spectrum from observations

---

<sup>8</sup>12  $\mu$ m flux from M 87 is 0.42 Jy (Knapp et al. 1990).

rather than from theories of particle acceleration is dictated by the fact, that such theories are still insufficiently developed to enable quantitative analysis. Next, we analyzed possible origin of the seed photons contributing to the inverse-Compton emission of the obtained electron spectrum, including nuclear jet radiation as well as ambient, stellar and circumstellar emission of the host galaxies, and discussed in detail spectral properties of the resulting  $\gamma$ -ray radiative output. The approach take into account effects connected with relativistic bulk motion of the emitting region, correcting earlier computations presented in the literature. We also clearly indicated limitation of the adopted approach due the Klein-Nishina regime effects. Other restrictions of the presented model are connected with only roughly evaluated galactic radiation fields and hardly known parameters of the hidden blazar radiation. Also, the effects of  $\gamma$ -ray absorption on CIB radiation are only shortly mentioned in this paper. However, even with all the aforementioned uncertainties, one can conclude that the detection of the high energy  $\gamma$ -ray emission by future ground-based and space telescopes from, at least, some of the FR I large scale jets is possible. Thus, the future observations will provide important constraints on the unknown jet parameters, like the magnetic field intensity and the jet Doppler factor, confirming or excluding possibilities of  $B \ll B_{eq}$  and  $\delta \neq 1$  discussed in the literature.

Our analysis provides constraints for  $\gamma$ -ray emission of the nearby FR I sources Centaurus A and M 87. For Centaurus A we predict measurable – by future  $\gamma$ -ray missions – fluxes at 10 GeV and 0.1 – 1 TeV photon energies due to comptonisation of the blazar radiation and the synchrotron self-Compton process, respectively. In the case of M 87 we show that recently detected VHE emission can result from comptonisation of the stellar and circumstellar infrared photons of the host galaxy.

Possibility that the *large scale* jets – and not the active centers – in these two FR I radio galaxies can dominate production of high energy  $\gamma$ -rays was not discussed previously in the literature. Some other authors, e.g. Bai and Lee (2001), Protheroe et al. (2003) or Donea and Protheroe (2003), suggested and studied production of very high energy  $\gamma$ -rays in the nuclear regions of the considered sources by the *small scale*, blazar-like jets. This constitutes the main difference with our work. Unfortunately, the angular resolution of the *IAC* systems will not allow for separation of the kiloparsec scale jet  $\gamma$ -ray radiation from the eventull core component. However, the core vs. the kpc-scale jet origin of  $\gamma$ -rays can be justified by studies of variability time scales.

The present work was supported by Komitet Badań Naukowych through the grant PBZ-KBN-054/P03/2001, by the Department of Energy contract to SLAC no. DE-AC3-76SF00515, and by NASA Chandra grants via SAO grant no. GO1-2113X. Authors acknowledge useful comments and suggestions by F.A. Aharonian and the anonymous referee.

### A. The observed and intrinsic jet luminosities

Let us consider an observer at rest in a frame  $K$ , and an emitting fluid comoving frame denoted by  $K'$ . Fluid velocity in the observer frame is  $\beta c$ , the appropriate Lorentz factor is  $\Gamma$ , and the Doppler factor for a given inclination angle  $\theta \equiv \cos^{-1} \mu$  with respect to the jet axis is  $\delta = [\Gamma (1 - \beta \mu)]^{-1}$ . In  $K$  frame the radiation intensity is  $I_\nu$  and the energy flux spectral density is  $S_\nu = \int I_\nu d\Omega$ , where  $\Omega = (\cos^{-1} \mu, \phi)$ . The total energy flux of the emission is  $S = \int S_\nu d\nu$ .

- As discussed by Lind and Blandford (1985) and Sikora et al. (1997), for a continuous (stationary) jet one has

$$S_\nu = \frac{\delta^2}{D^2} \int j'_{\nu'} dV \quad , \quad (\text{A1})$$

where  $j'_{\nu'}$  is an intrinsic emissivity of the fluid (i.e. the one measured in  $K'$ ),  $dV$  is the observed emitting volume element and  $D$  is the distance to the source. The observed isotropic luminosity is  $L = 4\pi D^2 S$ . Hence, with  $\nu = \delta \nu'$  and  $dV = dV'/\Gamma$ , one obtains

$$L = 4\pi \frac{\delta^3}{\Gamma} \frac{\partial L'}{\partial \Omega'} \quad , \quad (\text{A2})$$

where  $\partial L'/\partial \Omega' \equiv \int j' dV'$  is the fluid intrinsic radiative power emitted in a given direction  $\Omega' = (\cos^{-1} \mu', \phi')$ , and  $j' = \int j'_{\nu'} d\nu'$ . The total emitted power as measured in  $K'$  is then

$$L' = \oint \frac{\partial L'}{\partial \Omega'} d\Omega' = \frac{\Gamma}{\delta^3} L \quad , \quad (\text{A3})$$

where the last equality holds for the intrinsically isotropic emission.

- For a moving single blob of emitting plasma (with the observed volume element transforming as  $dV = \delta dV'$ ) the observed energy flux spectral density is

$$S_\nu = \frac{\delta^3}{D^2} \int j'_{\nu'} dV' \quad . \quad (\text{A4})$$

Hence

$$L = 4\pi \delta^4 \frac{\partial L'}{\partial \Omega'} \quad , \quad (\text{A5})$$

and in the case of intrinsically isotropic emission one obtains

$$L' = \oint \frac{\partial L'}{\partial \Omega'} d\Omega' = \frac{1}{\delta^4} L \quad . \quad (\text{A6})$$

Equations A3 and A6 specify the function  $g_{cj/mb}(\Gamma, \theta)$  defined in section 2.2 for the two considered jet models. Note, that in both cases, the ratio between intrinsic power and comoving volume of the emitting region is  $(L'/V') = (L/V) \delta^{-3}$ . Hence, the equipartition magnetic field is

$$B_{eq} \propto \left( \frac{L'_{syn}}{(\nu'_{eq, max})^{1/2} V'} \right)^{2/7} = \left( \frac{L_{syn}}{(\nu_{eq, max})^{1/2} V} \right)^{2/7} \delta^{-5/7} , \quad (\text{A7})$$

where  $\nu'_{eq, max} = \nu_{eq, max}/\delta$  is the maximum synchrotron frequency considered in derivation of  $B_{eq}$ . As a result, the equipartition magnetic field measured in the emitting region rest frame is related to the equipartition value computed for no beaming by relation

$$B_{eq} = B_{eq, \delta=1} \delta^{-5/7} . \quad (\text{A8})$$

This equation corrects the formula A7 of Harris and Krawczynski (2002).

## B. External radiation fields

Following the previous section, by  $K'$  we denote the inertial rest frame of the emitting matter of the kpc-scale jet. In the observer rest frame,  $K$ , the jet has bulk velocity  $\beta c$  and the respective bulk Lorentz factor  $\Gamma$ . Let us consider radiation external to the jet. Energy density of this emission measured in  $K'$  is

$$U'_{ext} = \frac{1}{c} \int_{\Delta\Omega'} I'_{ext} d\Omega' , \quad (\text{B1})$$

where  $I'$  is the jet comoving intensity of the external radiation and the integration is performed over the photons arrival directions. Defining next

$$\delta_{in} = [\Gamma (1 - \beta \cos \psi_{in})]^{-1} , \quad (\text{B2})$$

where  $\psi_{in}$  is the angle between external photons and the jet axis, one has  $I'_{ext} = I_{ext} \delta_{in}^{-4}$ ,  $d\Omega' = d\Omega \delta_{in}^2$  and thus

$$U'_{ext} = \frac{1}{c} \int_{\Delta\Omega'} I_{ext} \delta_{in}^{-2} d\Omega , \quad (\text{B3})$$

- For emission isotropic in  $K$  frame in vicinity of the kpc-scale jet, one obtains

$$U'_{ext} = \frac{I_{ext}}{c} \int_{4\pi} \delta_{in}^{-2} d\Omega = U_{ext} \Gamma^2 \left( 1 + \frac{\beta^2}{3} \right) , \quad (\text{B4})$$

where the last equality is due to  $U_{ext} = 4\pi I_{ext}/c$ .

- In a case of the external emission illuminating the jet from its base one has  $\psi_{in} \sim 0$  and hence

$$U'_{ext} = \frac{1}{c} \int_{\Delta\Omega'} \frac{I_{ext} d\Omega}{(2\Gamma)^2} \approx \frac{I_{ext} \Delta\Omega}{c} \frac{1}{(2\Gamma)^2} \quad , \quad (\text{B5})$$

where  $I_{ext} \Delta\Omega$  is approximately the emission energy flux received by the stationary observer located at the jet axis at the distance  $r$  from the considered source of the emission. The isotropic luminosity computed by such observer is therefore  $L_{ext}(0) = 4\pi r^2 I_{ext} \Delta\Omega$  and

$$U'_{ext} = \frac{L_{ext}(0)}{4\pi r^2 c} \frac{1}{(2\Gamma)^2} \quad . \quad (\text{B6})$$

### C. Starlight emission

Let us assume for the considered elliptical galaxies the spherical King-type stellar emissivity profile

$$j_{star}(\zeta) \propto (1 + \zeta^2)^{-3/2} \quad , \quad (\text{C1})$$

where  $\zeta \equiv r/r_c$ ,  $r \in (0, r_t)$  is a distance from the galactic center,  $r_c$  is a core radius and  $r_t$  is a terminal boundary radius of the stellar distribution (see section 2.2.3). With the assumed emissivity one can find the appropriate radiative intensity,  $I_{star}(\zeta, \zeta_t)$ , and next the mean intensity of the stellar radiation as a functions of  $r$

$$J_{star}(\zeta, \zeta_t) = \frac{1}{4\pi} \int I_{star}(\zeta, \zeta_t) d\Omega \quad , \quad (\text{C2})$$

where  $\zeta_t \equiv r_t/r_c$ . The analytical computations were performed by Tsai and Mathews (1995, see equation 26 therein). The energy density of the considered emission is simply  $U_{star}(\zeta, \zeta_t) = (4\pi/c) J_{star}(\zeta, \zeta_t)$ . Thus, knowing the central energy density of the starlight radiation,  $U_{star,C}$ , one can evaluate  $U_{star}$  at any distance from the galactic center as

$$U_{star}(\zeta, \zeta_t) = U_{star,C} \frac{J_{star}(\zeta, \zeta_t)}{J_{star}(0, \zeta_t)} \quad . \quad (\text{C3})$$

For ellipticals with the bolometric luminosities ranging from  $L_{bol} = 1.14 \cdot 10^{44}$  erg/s to  $L_{bol} = 1.23 \cdot 10^{45}$  erg/s, Tsai and Mathews (1995) estimated  $U_{star,C} = 1.2 \cdot 10^{-7} - 5.9 \cdot 10^{-9}$  erg/cm<sup>3</sup>,  $r_c = 0.04-0.77$  kpc and  $r_t = 44.4-123$  kpc, respectively (Table 1 therein). For these parameters, at the distance  $r = 1$  kpc from the galactic center, the bolometric starlight energy density computed accordingly to the equation C6 ranges from  $0.9 \cdot 10^{-9}$  erg/cm<sup>3</sup> up to  $3 \cdot 10^{-9}$  erg/cm<sup>3</sup>. Therefore, in this paper we take the average value  $U_{star}(1 \text{ kpc}) \sim 10^{-9}$  erg/cm<sup>3</sup>. We also assume for simplicity an approximately isotropic distribution of the discussed stellar emission in the galaxy rest frame at the kiloparsec scale.



### D. Anisotropy of the IC emission

Let us consider the above defined rest frames  $K$  and  $K'$ . The emitting fluid radiates through synchrotron and inverse-Compton processes, with intrinsic luminosities  $[\nu' L'_{\nu'}]_{syn}$  and  $[\nu' L'_{\nu'}]_{ic}$ , respectively. The jet magnetic field energy density is  $U'_B$ , and energy density of the seed photons as measured in  $K'$  is  $U'_{seed}$ . The ratio of the observed isotropic luminosities due to both considered processes is

$$\frac{[\nu L_{\nu}]_{ic}}{[\nu L_{\nu}]_{syn}} = \frac{4\pi g_{cj/mb}(\Gamma, \theta) \frac{\partial[\nu' L'_{\nu'}]_{ic}}{\partial\Omega'}}{4\pi g_{cj/mb}(\Gamma, \theta) \frac{\partial[\nu' L'_{\nu'}]_{syn}}{\partial\Omega'}} = \frac{\frac{\partial[\nu' L'_{\nu'}]_{ic}}{\partial\Omega'}}{\frac{\partial[\nu' L'_{\nu'}]_{syn}}{\partial\Omega'}} \quad (D1)$$

(Appendix A). Note, that in the above equation one compares the synchrotron and the inverse-Compton luminosities due to the electrons with the same energy  $\gamma \propto (\nu'_{syn}/B)^{1/2}$  and  $\gamma \propto (\nu'_{ic}/\nu'_{seed})^{1/2}$  (for example  $\gamma_{br}$  if break luminosities are considered). The intrinsic synchrotron power emitted in a given direction  $\Omega' \equiv (\cos^{-1} \mu', \phi')$  by isotropic electrons with the energy distribution  $n'_e(\gamma)$  within an uniformly filled volume  $V'$  is

$$\frac{\partial[\nu' L'_{\nu'}]_{syn}}{\partial\Omega'} = V' [\nu' j'_{\nu'}]_{syn} = \frac{1}{2} \frac{[\gamma n'_e(\gamma)]}{4\pi} V' |\dot{\gamma}|_{syn} mc^2 \quad , \quad (D2)$$

where  $|\dot{\gamma}|_{syn} mc^2 = \frac{4}{3} c\sigma_T U'_B \gamma^2$  is a mean rate of electron energy losses due to the synchrotron emission. It is not difficult to show (see below), that in the Thomson regime considered in this paper an analogous expression representing comptonisation of anisotropic (in  $K'$ ) seed photons is

$$\frac{\partial[\nu' L'_{\nu'}]_{ic}}{\partial\Omega'} = V' [\nu' j'_{\nu'}(\Omega')]_{ic} = \frac{1}{2} \frac{[\gamma n'_e(\gamma)]}{4\pi} V' |\dot{\gamma}(\Omega')|_{ic} mc^2 \quad , \quad (D3)$$

where  $|\dot{\gamma}(\Omega')|_{ic}$  denotes electron cooling rate due to the inverse-Compton emission. For the seed photons antiparallel (+) or parallel (–) in  $K'$  to the jet axis (if the seed photons are distributed isotropically around the relativistic jet, in its comoving frame their directions are almost antiparallel to the jet axis) one has

$$|\dot{\gamma}(\Omega')|_{ic(\pm)} = \frac{c\sigma_T}{mc^2} U'_{seed} \gamma^2 (1 \pm \mu')^2 \quad , \quad (D4)$$

while in the case of the isotropic (*iso*) distribution of the seed photons in the jet rest frame

$$|\dot{\gamma}(\Omega')|_{ic(iso)} = \frac{4}{3} \frac{c\sigma_T}{mc^2} U'_{seed} \gamma^2 \quad . \quad (D5)$$

Thus, the function  $f_{\pm/iso}(\Gamma, \theta)$  defined in equation 16 is

$$f_{\pm/iso}(\Gamma, \theta) = \begin{cases} \frac{3}{4} (1 \pm \mu')^2 & (\pm) \\ 1 & (iso) \end{cases} \quad . \quad (D6)$$

Transforming it to the observer rest frame, with  $\mu' = (\mu - \beta)/(1 - \beta\mu)$  one finally obtains  $f_{\pm/iso}(\Gamma, \theta)$  as given by the equation 17 (see also Dermer et al. 1992; Dermer 1995).

In order to find  $|\dot{\gamma}(\Omega')|_{ic}$  for the cases discussed above, let us evaluate the appropriate inverse-Compton emissivity  $[j'_{\nu'}]_{ic}$ . Here we write  $[\nu' j'_{\nu'}(\Omega')]_{ic} = mc^2 \epsilon'^2 \dot{n}'_{ic}(\epsilon', \Omega')$ , where the dimensionless photon energy  $\epsilon' \equiv h\nu'/m_e c^2$  and the photon emissivity is

$$\dot{n}'_{ic}(\epsilon', \Omega') = c \int d\epsilon'_{seed} \oint d\Omega'_{seed} \int d\gamma \oint d\Omega'_e (1 - \cos \chi') \sigma n'_{seed}(\epsilon'_{seed}, \Omega'_{seed}) n'_e(\gamma, \Omega'_e) . \quad (D7)$$

Here  $n'_{seed}(\epsilon'_{seed}, \Omega'_{seed})$  is a seed photon number density,  $n'_e(\gamma, \Omega'_e)$  is the electron energy distribution,  $\chi'$  is the angle between the electron and the seed photon direction,  $\sigma$  is the inverse-Compton scattering cross-section, and all quantities are measured in the emitting fluid rest frame  $K'$  (Dermer 1995).

- For the seed photons antiparallel (+) or parallel (–) in  $K'$  to the jet axis, assuming azimuthal symmetry and characteristic seed photon energy  $\langle \epsilon'_{seed} \rangle$ , one can write

$$n'_{seed}(\epsilon'_{seed}, \Omega'_{seed}) = \frac{1}{2\pi} n'_{seed} \delta(\epsilon'_{seed} - \langle \epsilon'_{seed} \rangle) \delta(\mu'_{seed} \pm 1) , \quad (D8)$$

where  $\Omega'_{seed} = (\cos^{-1} \mu'_{seed}, \phi'_{seed})$ . Thus, with the isotropic electron energy distribution  $n'_e(\gamma, \Omega'_e) = n'_e(\gamma)/4\pi$  and the Thomson scattering cross-section

$$\sigma = \sigma_T \delta[\epsilon' - \gamma^2 \epsilon'_{seed} (1 - \cos \chi')] \delta[\Omega' - \Omega'_e] \quad (D9)$$

(e.g., Dermer 1995), one obtains

$$\dot{n}'_{ic}(\epsilon', \Omega') = \frac{1}{2} \frac{c \sigma_T}{4\pi} n'_{seed} \left( \frac{1 \pm \mu'}{\epsilon' \langle \epsilon'_{seed} \rangle} \right)^{1/2} \int d\gamma n'_e(\gamma) \delta \left[ \gamma - \sqrt{\frac{\epsilon'}{\langle \epsilon'_{seed} \rangle (1 \pm \mu')}} \right] . \quad (D10)$$

This relation, with  $\gamma = \sqrt{\epsilon'/\langle \epsilon'_{seed} \rangle (1 \pm \mu')}$  and  $U'_{seed} = n'_{seed} \langle \epsilon'_{seed} \rangle mc^2$ , leads to  $\partial[\nu' L'_{\nu'}]_{ic}/\partial\Omega'$  given by expressions D3 and D4.

- For the seed photons isotropic in the jet comoving frame (*iso*), one can write

$$n'_{seed}(\epsilon'_{seed}, \Omega'_{seed}) = \frac{1}{4\pi} n'_{seed} \delta(\epsilon'_{seed} - \langle \epsilon'_{seed} \rangle) . \quad (D11)$$

Thus, with  $n'_e(\gamma, \Omega'_e) = n'_e(\gamma)/4\pi$  and the Thomson scattering cross-section

$$\sigma = \sigma_T \delta \left[ \epsilon' - \frac{4}{3} \gamma^2 \epsilon'_{seed} \right] \delta [\Omega' - \Omega'_e] \quad , \quad (D12)$$

one obtains

$$\begin{aligned} \dot{n}'_{ic(iso)}(\epsilon', \Omega') &= \frac{1}{2} \frac{c \sigma_T}{4\pi} n'_{seed} \left( \frac{3/4}{\epsilon' \langle \epsilon'_{seed} \rangle} \right)^{1/2} \\ &\int d\gamma n'_e(\gamma) \delta \left[ \gamma - \sqrt{\frac{\epsilon'}{\frac{4}{3} \langle \epsilon'_{seed} \rangle}} \right] \quad . \end{aligned} \quad (D13)$$

This, with  $\gamma = \sqrt{\epsilon'/\frac{4}{3} \langle \epsilon'_{seed} \rangle}$  and  $U'_{seed} = n'_{seed} \langle \epsilon'_{seed} \rangle mc^2$  leads to  $\partial[\nu' L'_{\nu'}]_{ic}/\partial\Omega'$  given by expressions D3 and D5.

### E. Break frequencies of the IC radiation

Let us consider the break frequency of the large scale jet inverse-Compton emission. Accordingly to the formalism presented in Appendix D, in the jet comoving frame a seed photon with the characteristic (break) frequency  $\nu'_{seed}$  is upscattered by the ultrarelativistic electron with Lorentz factor  $\gamma$  to the frequency  $\gamma^2 \nu'_{seed} (1 - \cos \chi')$ . For the electron break Lorentz factor  $\gamma_{br}$  one obtains the observed break frequency of the inverse-Compton emission

$$\nu_{ic(seed),br} = \gamma_{br}^2 \nu'_{seed} \delta (1 - \cos \chi') \quad . \quad (E1)$$

- For comptonisation of radiation distributed isotropically around the jet, one has  $\nu'_{seed} = \Gamma \nu_{seed}$  and  $1 - \cos \chi' = 1 + \mu'$ . Therefore

$$\nu_{ec(seed),br} = \gamma_{br}^2 \nu_{seed} \Gamma \delta (1 + \mu') = \gamma_{br}^2 \nu_{seed} \delta^2 \frac{(1 + \mu)}{(1 + \beta)} \quad . \quad (E2)$$

- In the case of seed photons illuminating kpc-scale jet from behind  $\nu'_{seed} = \nu_{seed}/\Gamma$  and  $1 - \cos \chi' = 1 - \mu'$ . Hence

$$\nu_{ec(seed),br} = \gamma_{br}^2 \nu_{seed} \frac{1}{\Gamma} \delta (1 - \mu') = \gamma_{br}^2 \nu_{seed} \delta^2 (1 - \mu) (1 + \beta) \quad . \quad (E3)$$

- For comptonisation of the isotropic (in  $K'$ ) radiation one has  $\nu'_{seed} = \nu_{seed}/\delta$  and the averaged  $\langle \nu'_{ic(seed)}/\nu'_{seed} \rangle = (4/3) \gamma^2$ . Therefore

$$\nu_{ic(seed),br} = \frac{4}{3} \gamma_{br}^2 \nu_{seed} \quad . \quad (E4)$$

Equations E2 - E4 specify the function  $h_{\pm/iso}(\Gamma, \theta)$  defined in section 2.3.

## REFERENCES

- Aharonian, F.A. 1998, in Proc. *Lepton-Photon Interactions*, World Scientific Publishing (astro-ph/9712089)
- Aharonian, F.A. 2001, in Proc. of the 27th ICRC, Hamburg, August 2001 (astro-ph/0112314)
- Aharonian, F.A. 2002, MNRAS, 332, 215
- Aharonian, F.A. et al. 2003, A&A, 403, L1
- Bai, J.M., and Lee, M.G. 2001, ApJ, 549, 173
- Bailey, J., Sparks, W.B., Hough, J.H., and Axon, D.J. 1986, Nature, 322, 150
- Bicknell, G.V., and Begelman, M.C. 1996, ApJ, 467, 597
- Biretta, J.A., Stern, C.P., and Harris, D.E. 1991, AJ, 101, 1632
- Biretta, J.A., Sparks, W.B., Macchetto, F., and Capetti, A. 1995, AAS, 187, 5016
- Biretta, J.A., Sparks, W.B., and Macchetto, F. 1999, ApJ, 520, 621
- Birkinshaw, M., Worrall, D.M., and Hardcastle, M.J. 2002, MNRAS, 335, 142
- Bregman, J.N. 1990, A&A Rev., 2, 125
- Bridle, A.H., and Perley, R.A. 1984, ARA&A, 22, 319
- Böhringer, H., Nulsen, P.E.J., Braun, R., and Fabian, A.C. 1995, MNRAS, 274, 67
- Böhringer, H., Belsole, E., Kennea, J., Matsushita, K., Molendi, S., Worrall, D.M., Mushotzky, R.F., Ehle, M., Guainazzi, M., Sakelliou, I., Stewart, G., Vestrand, W.T., and Dos Santos, S. 2001, A&A, 365, 181
- Burns, J.O., Feigelson, E.D., and Schreier, E.J. 1983, ApJ, 273, 128
- Capetti, A., Schreier, E.J., Axon, D., Young, S., Hough, J.H., Clark, S., Marconi, A., Macchetto, D., and Packham, C. 2000, ApJ, 544, 269
- Carilli, C.L., Harris, D.E., Pentericci, L., Rottgering, H.J.A., Miley, G.K., Kurk, J.D., and van Breugel, W. 2002, ApJ, 567, 781
- Cavallo, G., Horstman, H.M., and Muracchini, A. 1980, A&A, 86, 36
- Celotti, A., Ghisellini, G., and Chiaberge, M. 2001, MNRAS, 321, L1

- Chiaberge, M., Capetti, A., Celotti, A. 1999, A&A, 349, 77
- Chiaberge, M., Celotti, A., Capetti, A., and Ghisellini, G. 2000, A&A, 358, 104
- Chiaberge, M., Capetti, A., and Celotti, A. 2001, MNRAS, 324, 33
- Chiaberge, M., Gilli, R., Macchetto, F.D., Sparks, W.B., and Capetti, A. 2003, ApJ, 582, 645
- Clarke, D.A., Burns, J.O., and Norman, M.L. 1992, ApJ, 395, 444
- Coleman, C.S. and Bicknell, G.V. 1988 MNRAS, 230, 497
- Corbin, M.R., O’Neil, E., and Rieke, M.J. 2002, AJ, 124, 183
- Dermer, C.D. 1995, ApJ, 446, L63
- Dermer, C.D., Schlickeiser, R., and Mastichiadis, A. 1992, A&A, 256, 27
- Dermer, C.D., and Atoyan, A.M. 2002, ApJ, 568, 81
- Donea, A.-C., and Protheroe, R.J. 2003, PTPS, *submitted* (astroph/0303522)
- Fossati, G., Maraschi, L., Celotti, A., Comastri, A., and Ghisellini, G. 1998, MNRAS, 299, 433
- Golombek, D., Miley, G.K., and Neugebauer, G. 1988, AJ, 95, 26
- Gould, R.J., and Schreder, G. 1966, Phys. Rev. Lett., 16, 252
- Grindlay, J.E., Helmken, H.F., Brown, R.H., Davis, J., and Allen, L.R. 1975, ApJ, 197, 9
- Hardcastle, M.J., Birkinshaw, M., and Worrall, D.M. 2001, MNRAS, 326, 1499
- Hardcastle, M.J., Worrall, D.M., Birkinshaw, M., Laing, R.A., and Bridle, A.H. 2002, MNRAS, 334, 182
- Hardcastle, M.J., Worrall, D.M., Kraft, R.P., Forman, W.R., Jones, C., and Murray, S.S., 2003, ApJ, *accepted* (astroph/0304443)
- Harris, D.E., Biretta, J.A., and Junor, W. 1997, MNRAS, 284, 21
- Harris, D.E., and Krawczynski, H. 2002, ApJ, 565, 244
- Harris, D.E., Krawczynski, H., and Taylor, G.B. 2002a, ApJ, 578, 60

- Harris, D.E., Finoguenov, A., Bridle, A.H., Hardcastle, M.J., and Laing, R.A. 2002b, *ApJ*, 580, 110
- Harris, D.E., Biretta, J.A., Junor, W., Perlman, E.S., Sparks, W.B., and Wilson, A.S. 2003, *ApJ*, *accepted* (astro-ph/0302270)
- Hartman, R.C., Bertsch, D.L., Bloom, S.D., Chen, A.W., Deines-Jones, P., Esposito, J.A., Fichtel, C.E., Friedlander, D.P., Hunter, S.D., McDonald, L.M., Sreekumar, P., Thompson, D.J., Jones, B.B., Lin, Y.C., Michelson, P.F., Nolan, P.L., Tompkins, W.F., Kanbach, G., Mayer-Hasselwander, H.A., Mucke, A., Pohl, M., Reimer, O., Kniffen, D.A., Schneid, E.J., von Montigny, C., Mukherjee, R., and Dingus, B.L. 1999, *ApJS*, 123, 79
- Hauser, M.G., and Dwek, E. 2001, *ARA&A*, 39, 249
- Hawarden, T.G., Sandell, G., Matthews, H.E., Friberg, P., Watt, G.D., and Smith, P.A. 1993, *MNRAS*, 260, 844
- Jester, S. 2003, in *Proc. Relativistic jets in the Chandra and XMM Era*, *NewAR* (astro-ph/0212397)
- Jones, D.L., Tingay, S., Murphy, D., Meier, D., Jauncey, D., Reynolds, J., Tzioumis, A., Preston, R., McCulloch, P., Costa, M., Kembell, A., Nicolson, G., Quick, J., King, E., Lovell, J., Clay, R., Ferris, R., Gough, R., Sinclair, M., Ellingsen, S., Edwards, P., Jones, P., van Ommen, T., Harbison, P., and Migenes, V. 1996, *ApJ*, 466, 63
- Joy, M., Harvey, P.M., Tollestrup, E.V., Sellgren, K., McGregor, P.J., and Hyland, A.R. 1991, *ApJ*, 366, 82
- Kardashev, N.S. 1962, *Sov. Astr. A.J.*, 6, 317
- Karovska, M., Fabbiano, G., Nicastro, F., Elvis, M., Kraft, R.P., and Murray, S.S. 2002, *ApJ*, 577, 114
- Kino, M., Takahara, F., and Kusunose, M. 2002, *ApJ*, 564, 97
- Knapp, G.R., Bies, W.E., and van Gorkom, J.H. 1990, *AJ*, 99, 476
- Knapp, G.R., Gunn, J.E., and Wynn-Williams, C.G. 1992, *ApJ*, 399, 76
- Kneiske, T.M., Mannheim, K., and Hartmann, D.H. 2002, *A&A*, 386, 1

- Kraft, R.P., Forman, W., Jones, C., Kenter, A., Murray, S., Aldcroft, T., Elvis, M., Evans, I., Fabbiano, G., Isobe, T., Jerius, D., Karovska, M., Kim, D.-W., Prestwich, A., Primini, F., and Schwartz, D. 2000, *ApJ*, 531, L9
- Kraft, R.P., Forman, W.R., Jones, C., Murray, S.S., Hardcastle, M.J., and Worrall, D.M. 2002, *ApJ*, 569, 54
- Laing, R.A., Parma, P., de Ruiter, H.R., and Fanti, R. 1999, *MNRAS*, 306, 513
- Lind, K.R., and Blandford, R.D. 1985, *ApJ*, 295, 358
- Macchetto, F., Marconi, A., Axon, D.J., Capetti, A., Sparks, W., and Crane, P. 1997, *ApJ*, 489, 579
- Marconi, A., Schreier, E.J., Koekemoer, A., Capetti, A., Axon, D., Macchetto, D., and Caon, N. 2000, *ApJ*, 528, 276
- Marshall, H.L., Miller, B., Davis, D., Perlman, E., Wise, M., Canizares, C., and Harris, D. 2002, *ApJ*, 564, 683
- Meisenheimer, K., Röser, H.-J., and Schlötelburg, M. 1996, *A&A*, 307, 61
- von Montigny, C., Bertsch, D., Chiang, J., Dingus, B., Esposito, J., Fichtel, C., Fierro, J., Hartman, R., Hunter, S., Kanbach, G., Kniffen, D., Lin, Y., Mattox, J., Mayer-Hasselwander, H., Michelson, P., Nolan, P., Radecke, H., Schneid, E., Sreekumar, P., Thompson, D., and Willis, T. 1995, *ApJ*, 440, 525
- Morganti, R., Robinson, A., Fosbury, R.A.E., di Serego Alighieri, S., Tadhunter, C.N., and Malin, D.F. 1991, *MNRAS*, 249, 91
- Morini, M., Anselmo, F., and Molteni, D. 1989, *ApJ*, 347, 750
- Nikishov, A.I. 1962, *Sov. Phys. JETP*, 14, 393
- Owen, F.N., Hardee, P.E., and Cornwell, T.J. 1989, *ApJ*, 340, 698
- Owen, F.N., Eilek, J.A., and Kassim, N.E. 2000, *ApJ*, 543, 611
- Packham, C., Hough, J.H., Young, S., Chrysostomou, A., Bailey, J.A., Axon, D.J., Ward, M.J. 1996, *MNRAS*, 278, 406
- Perlman, E.S., Biretta, J.A., Zhou, F., Sparks, W.B., and Macchetto, F.D. 1999, *AJ*, 117, 2185

- Perlman, E.S., Biretta, J.A., Sparks, W.B., Macchetto, F.D., and Leahy, J.P. 2001, *ApJ*, 551, 206
- Protheroe, R.J. and Meyer, H. 2000, *Phys. Rev. B*, 493, 1
- Protheroe, R.J., Donea, A.-C., and Reimer, A. 2003, *APh*, 19, 559
- Punch, M., Akerlof, C., Cawley, M., Chantell, M., Fegan, D., Fennell, S., Gaidos, J., Hagan, J., Hillas, A., Jiang, Y., Kerrick, A., Lamb, R., Lawrence, M., Lewis, D., Meyer, D., Mohanty, G., O’Flaherty, K., Reynolds, P., Rovero, A., Schubnell, M., Sembroski, G., Weekes, T., and Wilson, C. 1992, *Nature*, 358, 477
- Quinn, J., Akerlof, C., Biller, S., Buckley, J., Carter-Lewis, D., Cawley, M., Catanese, M., Connaughton, V., Fegan, D., Finley, J., Gaidos, J., Hillas, A., Lamb, R., Krennrich, F., Lessard, R., McEnery, J., Meyer, D., Mohanty, G., Rodgers, A., Rose, H., Sembroski, G., Schubnell, M., Weekes, T., Wilson, C., and Zweerink, J. 1996, *ApJ*, 456, 83
- Reynolds, C.S., Heinz, S., Fabian, A.C., and Begelman, M.C. 1999 *ApJ*, 521, 99
- Rowell, G.P., Dazeley, S.A., Edwards, P.G., Gunji, S., Hara, T., Holder, J., Kawachi, A., Kifune, T., Matsubara, Y., Mizumoto, Y., Mori, M., Muraishi, H., Muraki, Y., Naito, T., Nishijima, K., Ogio, S., Patterson, J.R., Roberts, M.D., Sako, T., Sakurazawa, K., Susukita, R., Tamura, T., Tanimori, T., Thornton, G.J., Yanagita, S., Yoshida, T., and Yoshikoshi, T. 1999, *APh*, 11, 217
- Sahayanathan, S., Misra, R., Kembhavi, A.K., and Kaul, C.L., 2003, *ApJ*, 588, 77
- Scarpa, R., and Urry, C.M. 2002, *NewAR*, 46, 405
- Schreier, E.J., Feigelson, E., Delvaille, J., Giacconi, R., Grindlay, J.E., Schwartz, D., and Fabian, A. 1979, *ApJ*, 234, 39
- Schreier, E.J., Gorenstein, P., and Feigelson, E.D. 1982, *ApJ*, 261, 42
- Schreier, E.J., Capetti, A., Macchetto, F., Sparks, W.B., and Ford, H.J. 1996, *ApJ*, 459, 535
- Schreier, E.J., Marconi, A., Axon, D.J., Caon, N., Macchetto, D., Capetti, A., Hough, J.H., Young, S., and Packham, C. 1998, *ApJ*, 499, 143
- Sikora, M., Madejski, G., Moderski, R., and Poutanen, J. 1997, *ApJ*, 484, 108
- Sikora, M., and Madejski, G. 2002, in *Proc. 2nd KIAS Astrophysics Workshop*, World Scientific Publishing (astro-ph/0112231)



- Sparks, W.B., Golombek, D., Baum, S.A., Biretta, J., de Koff, S., Macchetto, F., McCarthy, P., and Miley, G.K. 1995, *ApJ*, 450, L55
- Sparks, W.B., Biretta, J.A., and Macchetto, F. 1996, *ApJ*, 473, 254
- Sreekumar, P., Bertsch, D.L., Dingus, B.L., Esposito, J.A., Fichtel, C.E., Fierro, J., Hartman, R.C., Hunter, S.D., Kanbach, G., Kniffen, D.A., Lin, Y.C., Mayer-Hasselwander, H.A., Mattox, J.R., Michelson, P.F., von Montigny, C., Mukherjee, R., Nolan, P.L., Schneid, E., Thompson, D. J., and Willis, T.D. 1996, *ApJ*, 464, 628
- Sreekumar, P., Bertsch, D.L., Hartman, R.C., Nolan, P.L., and Thompson, D.J. 1999, *APh*, 11, 221
- Stawarz, L., and Ostrowski, M. 2002, *ApJ*, 578, 763
- Stecker, F.W., de Jager, O.C., and Salamon, M.H. 1992, *ApJ*, 390, 49
- Steinle, H., Bennett, K., Bloemen, H., Collmar, W., Diehl, R., Hermsen, W., Lichti, G.G., Morris, D., Schonfelder, V., Strong, A.W., and Williams, O.R. 1998, *A&A*, 330, 97
- Tavecchio, F., Maraschi, L., Sambruna, R.M. and Urry, C.M. 2000, *ApJ*, 544, 23
- Tavecchio, F., Ghisellini, G., and Celotti, A. 2003, *A&A*, 403, 83
- Tsai, J.C., and Mathews, W.G. 1995, *ApJ*, 448, 84
- Tsai, J.C., and Mathews, W.G. 1996, *ApJ*, 468, 571
- Tsvetanov, Z.I., Hartig, G.F., Ford, H.C., Dopita, M.A., Kriss, G.A., Pei, Y.C., Dressel, L.L., and Harms, R.J. 1998, *ApJ*, 493, 83
- Urry, C.M., and Padovani, P. 1995, *PASP*, 107, 803
- Weekes, T.C., Fazio, G., Helmken, H., O’Mongain, E., and Rieke, G. 1972 *ApJ*, 174, 165
- Völk, H.J. 2003, in *Proc. Astronomy, Cosmology and Fundamental Physics*, ESO Astrophysics Symposia (astroph/0210297)
- Whysong, D., and Antonucci, R. 2001, *ApJ*, (astroph/0106381)
- Wilson, A.S. and Yang, Y. 2002, *ApJ*, 568, 133
- Worrall, D.M., Birkinshaw, M., and Hardcastle, M.J. 2001, *MNRAS*, 326, L7

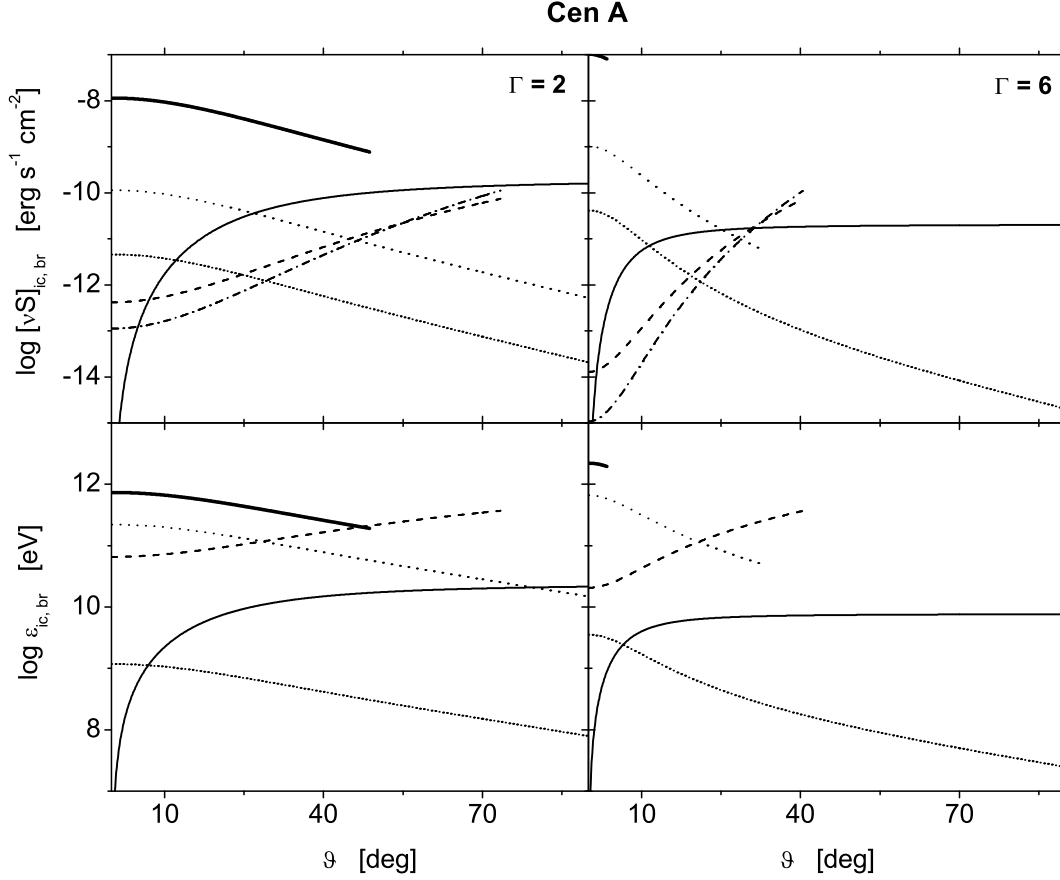


Fig. 1.— High energy  $\gamma$ -ray emission of the Centaurus A large scale jet region A1 - A4 for different jet viewing angles  $\theta$ ,  $B = B_{eq}$  and the bulk Lorentz factors  $\Gamma = 26$ . Other parameters are discussed in Section 3.1. The upper panels show the observed IC fluxes, while the lower panels indicate the respective observed photon break energies. The solid lines correspond to the EC(bl) emission, the dotted lines to the EC(dust) process, the short-dotted line to the EC(CMB) radiation, thick solid line to the EC(star) emission and, finally, the dashed and dash-dotted lines to the SSC radiation of a continuous jet and moving blob, respectively. The lines are presented only till the Klein-Nishina limit.

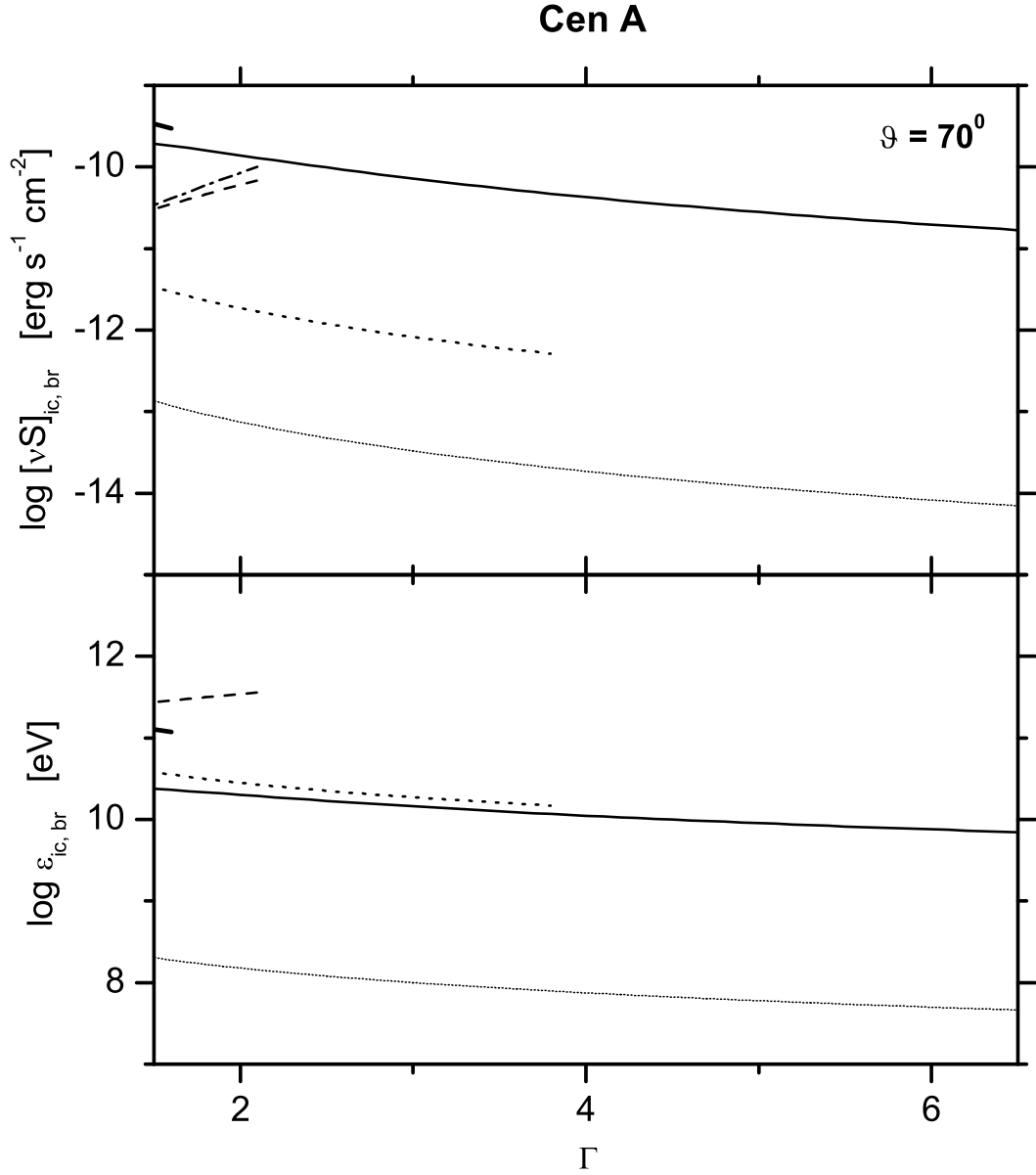


Fig. 2.— High energy  $\gamma$ -ray emission of the Centaurus A large scale jet region A1 - A4 in function of the bulk Lorentz factor  $\Gamma$ , for the jet viewing angle  $\theta = 70^\circ$  and the magnetic field  $B = B_{eq}$ . The other parameters and description of the presented curves are the same as in Figure 1.

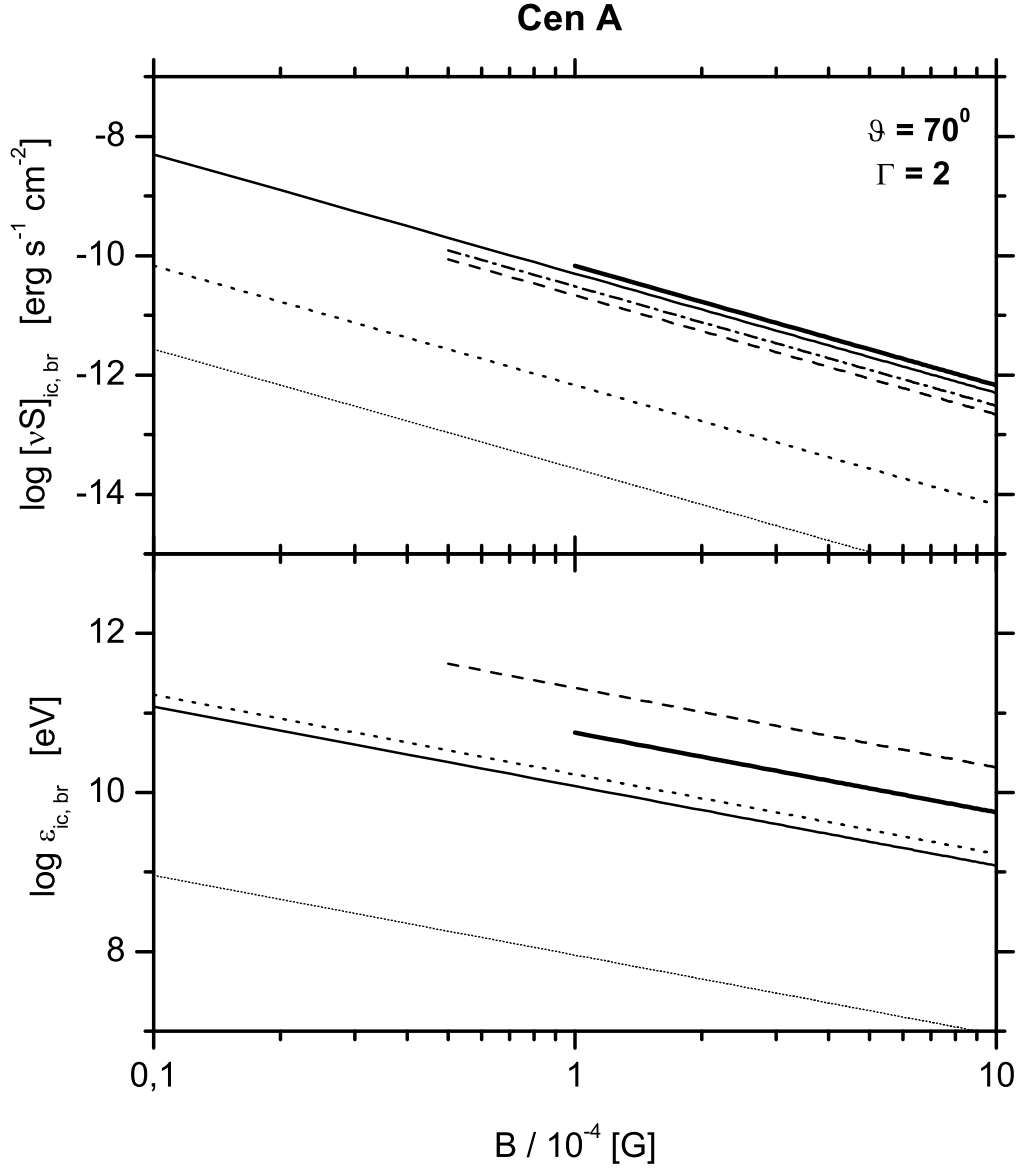


Fig. 3.— High energy  $\gamma$ -ray emission of the Centaurus A large scale jet region A1 - A4 in function of the magnetic field  $B$ , for the jet viewing angle  $\theta = 70^\circ$  and the bulk Lorentz factor  $\Gamma = 2$ . The other parameters and description of the presented curves are the same as in Figure 1.

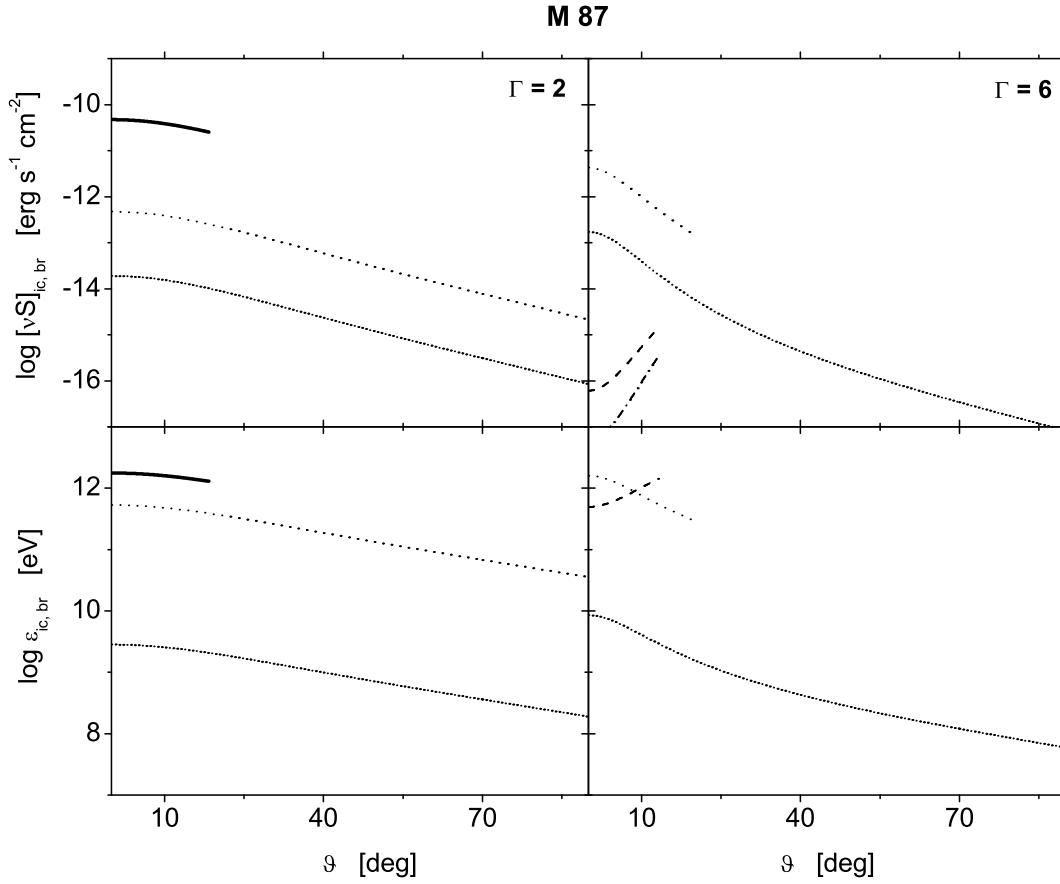


Fig. 4.— High energy  $\gamma$ -ray emission of the M 87 knot A for different jet viewing angles  $\theta$ ,  $B = B_{eq}$  and the bulk Lorentz factors  $\Gamma = 26$ . The other parameters are discussed in Section 3.2. Description of the presented curves is the same as in Figure 1.

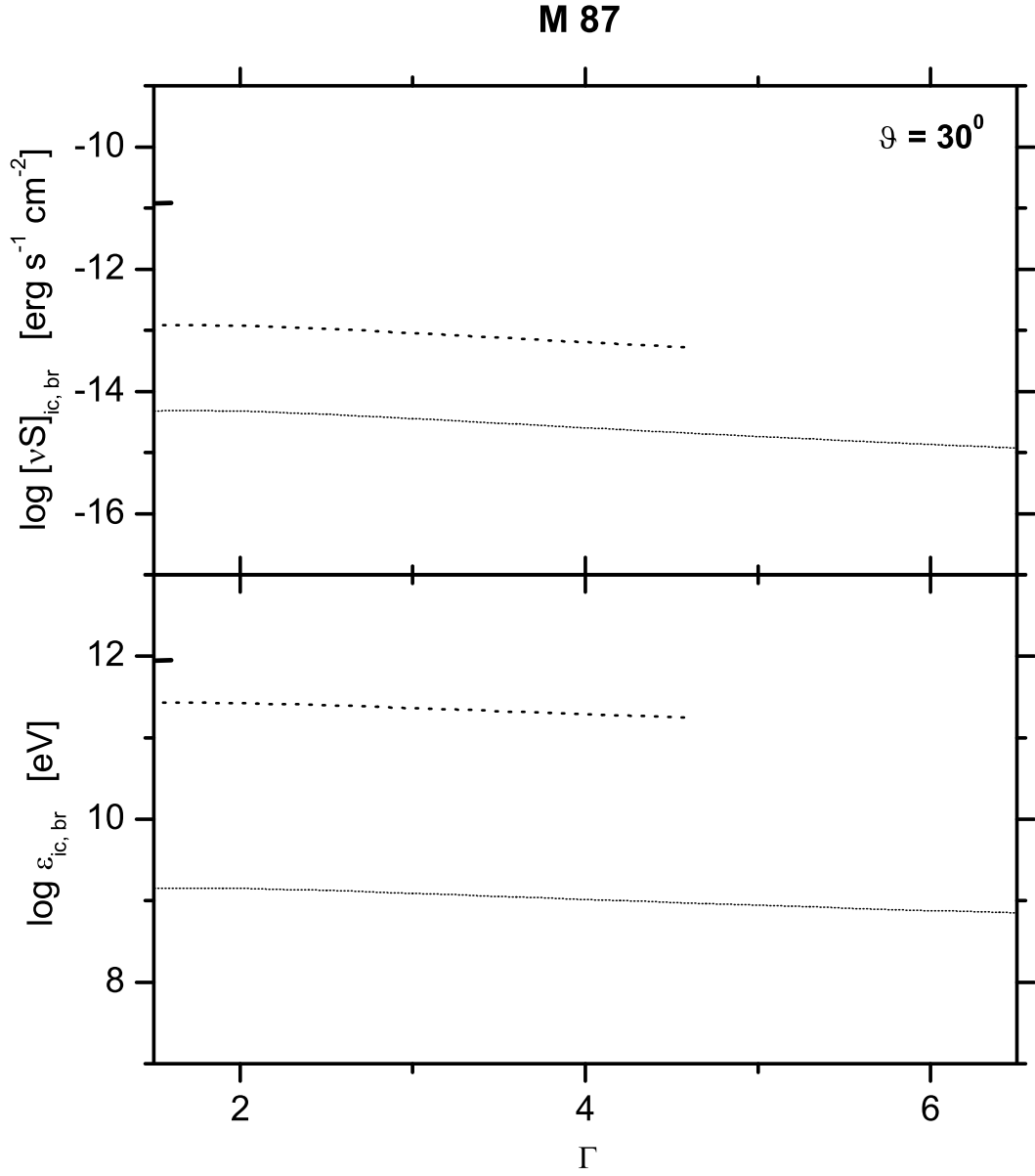


Fig. 5.— High energy  $\gamma$ -ray emission of the M 87 knot A in function of the bulk Lorentz factor  $\Gamma$ , for the jet viewing angle  $\theta = 30^{\circ}$  and the magnetic field  $B = B_{eq}$ . The other parameters and description of the presented curves are the same as in Figure 4.

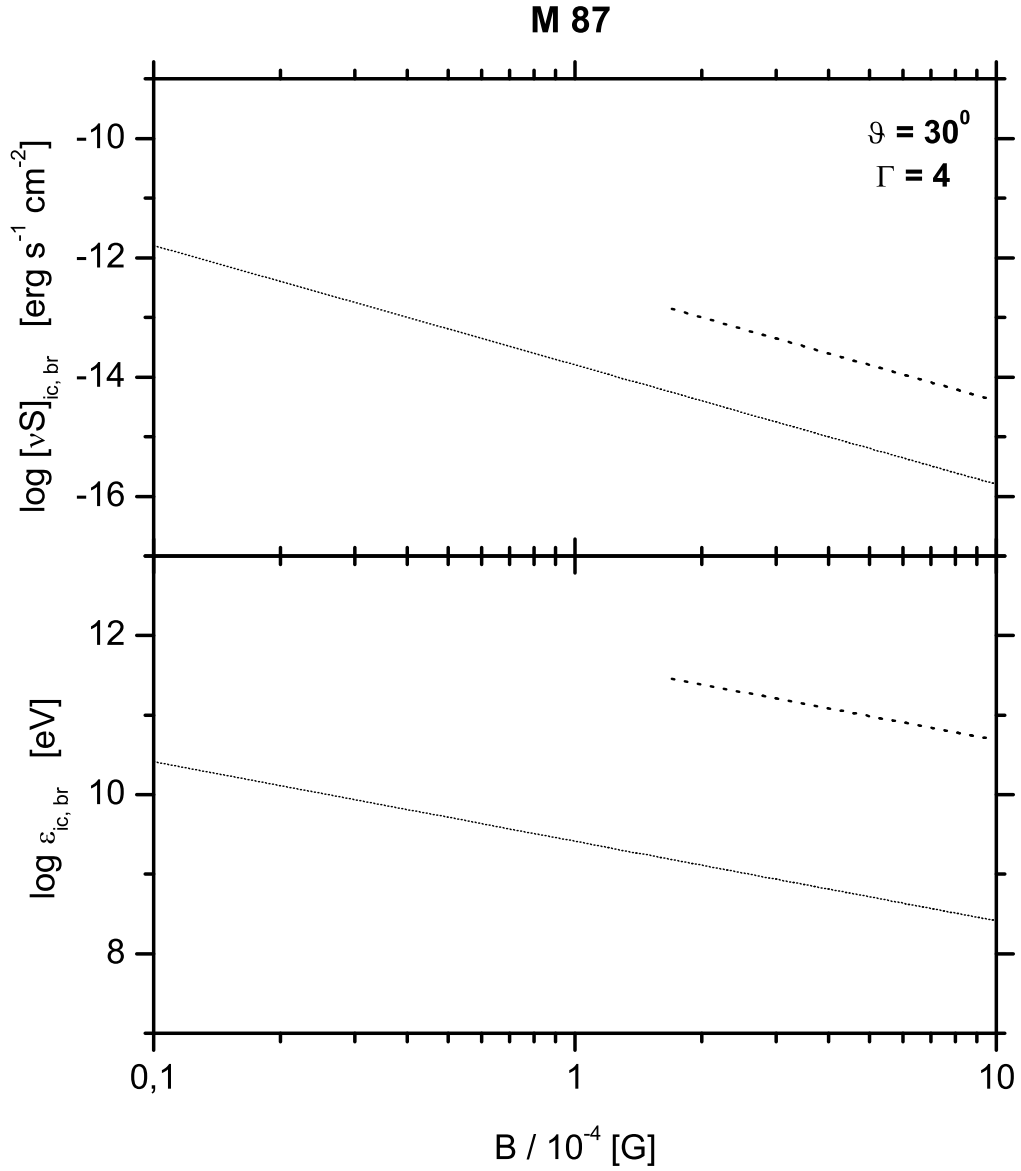


Fig. 6.— High energy  $\gamma$ -ray emission of the M 87 knot A in function of the magnetic field  $B$ , for the jet viewing angle  $\theta = 30^{\circ}$  and the bulk Lorentz factor  $\Gamma = 4$ . The other parameters and description of the presented curves are the same as in Figure 4.